Soil & Tillage Research 241 (2024) 106101

Contents lists available at ScienceDirect

Soil & Tillage Research

journal homepage: www.elsevier.com/locate/still

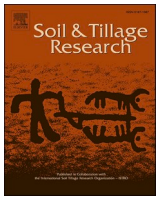

Biochar from cashew residue enhances silicon adsorption and reduces cohesion and mechanical resistance at meso- and micro-structural scales of soil with cohesive character

Ícaro Vasconcelos do Nascimento [a,1,*], Emanuela Barbosa dos Santos [a], Angélica da Silva Lopes [a], Alexandre dos Santos Queiroz [a], Crisanto Dias Teixeira Filho [a], Ricardo Espíndola Romero [a], Mirian Cristina Gomes Costa [a], Odair Pastor Ferreira [b], Antônio Gomes Souza Filho [c], Laís Gomes Fregolente [c], Francisca Gleiciane da Silva [a], Arthur Prudêncio de Araujo Pereira [a], Helon Hébano de Freitas Sousa [a], Viviane Sobucki [d], José Miguel Reichert [e], Jaedson Cláudio Anunciato Mota [a]

[a] Federal University of Ceará (UFC), Soil Science Department, 2977, Av. Mister Hull, Campus do Pici, Fortaleza, CE 60356-001, Brazil
[b] State University of Londrina (UEL), Department of Chemistry, Highway Celso Garcia Cid (445) - km 380, Londrina, PR 86050-482, Brazil
[c] Federal University of Ceará (UFC), Department of Physics, Campus do Pici, Fortaleza, CE 60455-900, Brazil
[d] Federal University of Santa Maria (UFSM), Soils Department, Av. Roraima 1000, Rural Sciences Center, 42, Santa Maria, RS 97105-900, Brazil
[e] Federal University of Pernambuco (UFPE), Nuclear Engineering Department, Av. Prof. Luiz Freire, 1000, Recife, PE 50.740-545, Brazil

ARTICLE INFO

Keywords:
Soil conditioners
Coastal Tablelands
Densified soils
Silicon
Amorphous silica
Soil microstructure

ABSTRACT

Horizons with cohesive character impose physical restraints on plant development, particularly when it occurs near the soil surface. Howbeit, the genesis of cohesive character in soils is associated with temporary and reversible cementation by amorphous silica. Thus, we hypothesized that the biochar obtained from residues from cashew processing would improve soil porosity and promotes silicon adsorption, consequently reducing cohesion and mechanical resistance while improving the physical quality of soils with cohesive character. We collected soil samples with deformed structure from the Bt1 horizon of a Typic Haplustult with cohesive character in northeast Brazil. These samples were used to prepare test substrates by combining air-dried and sieved soil samples and biochar at application rates of 0, 5, 10, 20, and 40 Mg ha^{-1}. All the samples in each treatment underwent ten cycles of wetting and drying (one cycle per week) to allow the manifestation of the cohesive character. Subsequently, we assessed silicon adsorption capacity, soil bulk density, porosity, soil penetration resistance, tensile strength, and rheometric properties. In the 5 and 10 Mg ha^{-1} doses, the physical quality remained like the control treatment (0 Mg ha^{-1}). The 20 and 40 Mg ha^{-1} doses resulted in increased soil silicon adsorption capacity (+7.6 and +15.3%, respectively), total porosity (+2.0 and +1.9%, respectively), and macroporosity (+14.6 and +15.3%, respectively), compared to the treatment without biochar. Conversely, these doses led to a reduction in soil bulk density (-0.1 and −0.8%, respectively), penetration resistance (-16.2 and −16.1%, respectively), tensile strength (-24.2 and −36.5%, respectively), deformation at the end of the linear viscoelastic range (-6.3 and −10.5%, respectively), shear stress at the end of the linear viscoelastic range (-16.4 and −26.9%, respectively), and maximum shear stress (-13.7 and −22.3%, respectively). In conclusion, the application of biochar improved soil porosity and promoted silicon adsorption, thus reducing the bulk density, cohesion, and mechanical resistance, enhancing the physical quality of soils with cohesive character, especially for doses of 20 and 40 Mg ha^{-1}.

* Corresponding author.
E-mail address: icaro_agro@hotmail.com (Í.V. Nascimento).
[1] (ORCiD: 0000-0001-5222-3589)

https://doi.org/10.1016/j.still.2024.106101
Received 20 October 2023; Received in revised form 14 March 2024; Accepted 24 March 2024

1. Introduction

Soil quality refers to the ability of soil to perform different functions in natural and managed ecosystems (Doran and Parkin, 1994). These functions include supporting the development of plants and animals, maintaining or improving the water quality, providing mechanical support for structures, as well as promoting the health of humans, plants, and animals, sequestering atmospheric carbon, and serving as a habitat for various organisms (Karlen et al., 1997; Lal, 2016; Seifu and Elias, 2018). From the perspective of soil physical quality, penetration resistance stands out as an indicator because it directly influences root growth and, consequently, plant development and productivity (Valadão Junior et al., 2014). Another indicator is tensile strength, which can be used to infer the effect of soil use and management practices on soil quality (Oliveira et al., 2020).

Soil structure, especially at the microscale, depends on electrostatic interactions between particles and the presence of binding agents (Markgraf et al., 2006). Therefore, in addition to evaluation at the mesoscale (samples between 100 and 300 cm^3), soil mechanical resistance can be assessed at the microstructural scale (samples between 7 and 10 cm^3) through rheometry (Holthusen et al., 2012a, 2012b). It is worth mentioning that, as classical fluid mechanics cannot describe the deformation and flow process for all materials, rheology comes to be considered when the flow properties are more complex than those of a simple fluid (Markgraf, 2011).

Soils with cohesive character have limitations in their physical quality (Mota et al., 2018). These soils are characterized by densified subsurface pedogenic horizons, found at a depth between 0.30 and 0.70 m, that are very to extremely hard when dry and friable or firm when moist, with massive or weakly aggregated structure (Lima Neto et al., 2009; Santos et al., 2018). One of the hypotheses for the genesis of these horizons is densification through processes of reversible polymerization and precipitation of low crystallinity siliceous and silico-aluminous compounds associated with wetting and drying cycles (Araújo Filho et al., 2001). The primary consequence of this process is a more compact arrangement of soil particles, imposing physical limitations on root development and plant growth (Marques et al., 2021).

As most of the metabolically active plant roots are concentrated in the topsoil (Tang et al., 2023), the presence of cohesive horizons near the surface can hinder the productive potential of the plants cultivated on these soils. This happens because of the increase of both bulk density and root penetration resistance, as well as the decrease in total porosity, affecting the water and air flow (Giarola et al., 2001), particularly in dry soil when the cohesion increases (Mota et al., 2021; Queiroz et al., 2023). So, management of this type of limitation is necessary in high-technology agricultural systems, in which soil conditions are optimized to maximize crop productivity.

The costs of subsoiling operations tend to be high in areas with cohesive horizons (Corrêa et al., 2023). Therefore, in situations where the cohesive horizon is close to the surface, one strategy to improve the soil physical quality and promote plant development is the use of soil conditioners. These materials can be incorporated into the soil at depths of up to 0.40 m in conventional systems, but with the possibility of reaching up to 0.80 m in depth (Campos et al., 2022). One conditioner that has gained prominence is biochar, obtained by the pyrolysis of biomass in a limited oxygen atmosphere (Nascimento et al., 2023). High specific surface area and high density of negative surface charges characterize biochar, which allow the conditioner to adsorb water and nutrients to plants (Yang et al., 2019). The application of biochar also improves soil aeration and microbial activity and contributes to carbon sequestration due to the high recalcitrance of carbon in its structure (Elkhlifi et al., 2023; Li and Tasnady, 2023; Luo et al., 2023; Nascimento et al., 2023).

The impact of biochar on the biogeochemical cycle of silicon (Si) is still not clear, thus showing the importance of studying the relationship between biochar and Si, which is the second most abundant element in the Earth's crust (Savant et al., 1999; Sommer et al., 2006; Wang et al., 2020). Once incorporated into the soil or reaching the subsurface layer due to vertical mobility (Zhang et al., 2023), biochar can adsorb silicic acid (H_4SiO_4) into its porous structure (Wang et al., 2018). The effect is more pronounced for biochar derived from materials with low Si content, which can act as Si sinks in the soil (Wang et al., 2019). Hence, biochar with low Si content could adsorb the element from the solution and alleviate mechanical constraints on plant development in soils with cohesive character.

There are no records of cashew trees (Anacardiaceae, *Anacardium occidentale* L.) being silicon accumulators, a characteristic primarily associated with monocots of the Poaceae family (Hodson et al., 2005), and some dicots like those in the Curcubitaceae family (Ma and Takahashi, 2002). Therefore, the use of cashew tree residues allows the production of biochar with low silicon content, favoring the adsorption of the element over its release. Additionally, cashew production is concentrated in the Northeast Region of Brazil (Oliveira and Ipiranga, 2011), where this study was conducted, and cashew farming faces significant challenges related to waste management (Kannan et al., 2021), such as the destination of the bagasse resulting from the processing of the pseudo fruit.

So, we hypothesized that the application of biochar obtained from the pyrolysis of residues from cashew processing improves soil porosity and promotes silicon adsorption, thus reducing cohesion and mechanical resistance, and improving the physical quality of soil with cohesive character. The objectives of this study were to assess if biochar application improves soil silicon adsorption capacity and reduces soil cohesion and resistance and to identify the most effective biochar dose for improving the physical quality of soils with cohesive character.

2. Material and methods

2.1. Soil sample collection

Soil samples were collected in an experimental area of the Federal University of Ceará, located in Fortaleza, Ceará, Brazil (Fig. 1A). Fortaleza has a tropical wet-dry climate – Aw (Koppen, 1918). The studied area (3°44'41.6"S, 38°34'51.5"W, Fig. 1B) has not undergone anthropogenic intervention in the last 15 years, remaining fallow. The soil was classified as an Argissolo Amarelo Eutrocoeso típico (Santos et al., 2018), Typic Haplustult (Soil Survey Staff, 2022), or Haplic Lixisol (IUSS Working Group WRB, 2022). The characterization of the studied soil, according to Vieira (2013), is presented in Table 1. The soil samples with deformed structure were collected in the center of the Bt1 horizon with cohesive character (0.96 – 1.45 m) for the assembly of test specimens. The studied horizon has 45.9% sand, 10.1% silt, and 44.0% clay, belonging to the sandy clay textural class. The samples were air-dried to equilibrium with ambient moisture, then crushed using a roller and sieved with a mesh opening of 2 mm to obtain air-dried fine earth.

2.2. Preparation of test specimens, treatments, and experimental design

The experimental design was completely randomized, with five treatments and five replicates, totaling 25 experimental units per treatment. Test specimens were prepared using air-dried soil samples and biochar obtained from the pyrolysis of cashew processing residues, considering the treatments 0 (B0), 5 (B5), 10 (B10), 20 (B20), and 40 (B40) Mg ha^{-1}. To produce the biochar, the cashew bagasse was dried in an oven (40°C for 24 hours). Then, the biomass was ground and sieved through a mesh with an opening of 2 mm. Slow pyrolysis was carried out in a tubular furnace (FTHI/20, EDG), at 550°C for 90 minutes, under a moderate flow of nitrogen. The biochar characteristics were previously described by Fregolente et al. (2023), however, the elemental composition and ashes content of biochar are presented in Table 2. As explained in the introduction, cashew residues were chosen due to their availability in the given region as well as due to their low Si content.

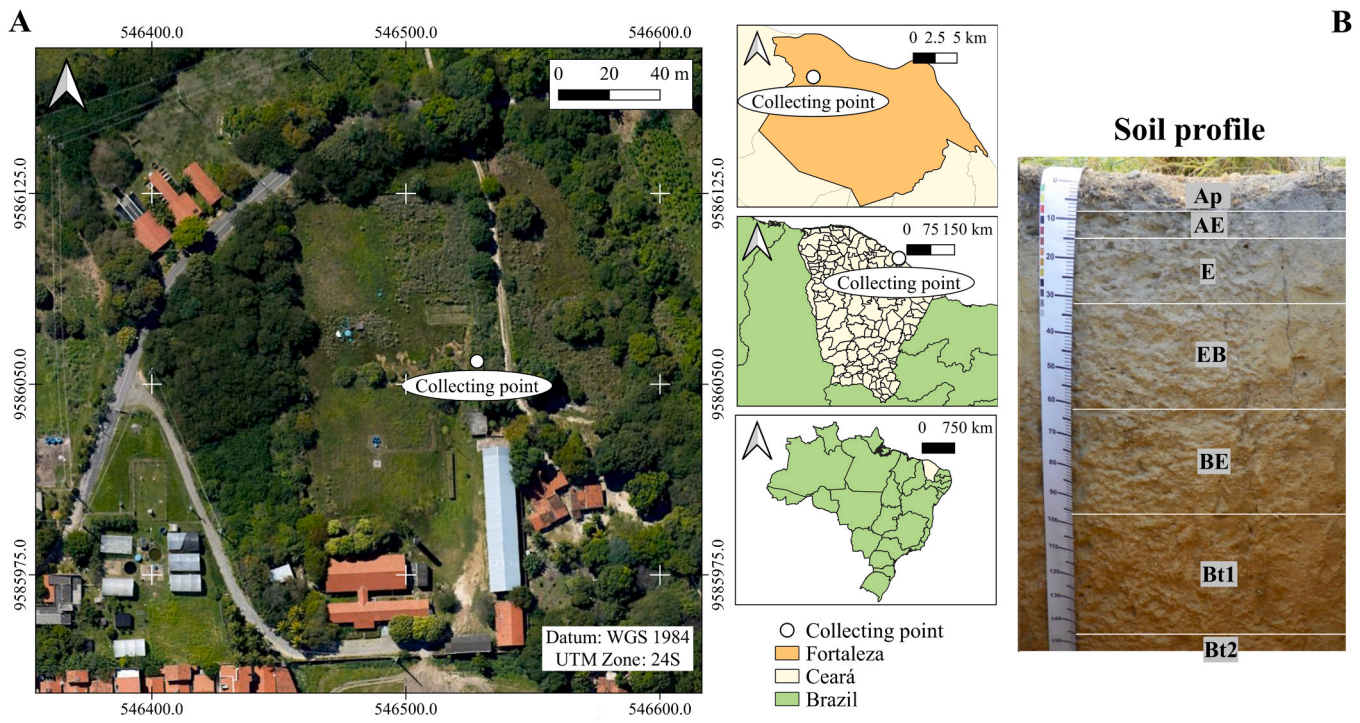

Fig. 1. Location of collecting point – Fortaleza, Ceará, Brazil (A). Profile of the Argissolo Amarelo Eutrocoeso (Typic Haplustult) (B). Soil profile photo: Vieira (2013).

Table 1
Characterization of the soil.

Horizon	Depth (cm)	Exchangeable cations ($cmol_c\ kg^{-1}$)						SB	CEC	BS (%)	pH	Granulometric fractions (%)		
		Ca^{2+}	Mg^{2+}	K^{+}	Na^{+}	Al^{3+}	H^{+}	($cmol_c\ kg^{-1}$)				Sand	Silt	Clay
Ap	0–8	3.0	4.4	0.36	0.37	0.2	2.0	8.13	10.33	79	6.0	82.6	10.9	6.5
AE	8–15	2.0	3.8	0.21	0.37	0.2	1.2	6.39	7.79	82	6.2	82.3	9.0	8.7
E	15–32	1.4	2.8	0.24	0.36	0.4	1.8	4.79	6.99	69	6.3	81.0	6.6	12.4
EB	32–62	1.4	3.2	0.30	0.43	0.4	1.8	5.33	7.53	71	6.3	70.6	7.8	21.6
BE	62–96	2.2	2.0	0.39	0.41	0.6	1.5	5.00	7.10	70	6.3	61.4	9.4	29.2
Bt1	96–145	1.6	3.8	0.40	0.43	0.6	1.6	6.23	8.43	74	6.3	45.9	10.1	44.0
Bt2	145–190+	1.8	3.0	0.17	0.46	0.4	1.6	5.43	7.43	73	6.4	47.9	10.8	41.3

SB – Sum of bases. CEC – Cation exchange capacity. BS – Base saturation. pH measured in water.
Source: Vieira (2013).

Table 2
Biochar elemental composition, ash content, and O/C and H/C atomic ratios.

Variables	
Specific surface area ($m^2\ g^{-1}$)	70.0
C (%)	80.1
H (%)	2.5
N (%)	2.8
S (%)	0.2
O (%)	10.8
Ash (%)	3.6
O/C Atomic ratio	0.10
H/C Atomic ratio	0.38

Source: Fregolente et al. (2023).

Using the molybdenum blue colorimetric method (Kilmer, 1965), we measured a silicon adsorption capacity of the final biochar of 2.3 mg g^{-1}. For methodology, see section 3.2.1 "Silicon adsorption capacity".

At the time of preparing the test samples, the doses were transformed into mass percentages. For this, the mass of biochar from the respective treatment and the mass of soil that occupies the area of 1 ha were considered. The soil mass was obtained using the thickness and bulk density data from the cohesive horizon where the soil was collected (thickness = 0.49 m; bulk density = 1550 kg m^{-3}). For example, for the dose of 40 Mg ha^{-1}, there is 40,000 kg of biochar for 7595,000 kg of soil. This results in a biochar-to-soil ratio of 0.005–1, which is equivalent to 0.5% w/w. Before preparing the test specimens (soil with biochar, in metallic rings measuring approximately 100 cm^3 – internal diameter and height of approximately 5 cm), the soil was carefully mixed with the biochar considering the treatments described previously. For this purpose, we added soil and biochar into a plastic bag which was then sealed. Subsequently, the plastic bag was shaken to ensure the mixture was homogenized.

Initially, two sets of samples were prepared: the first for the evaluation of penetration resistance and the collection of material for silicon adsorption trials; and the second for the evaluation of total porosity, macroporosity, and microporosity. Soil bulk density was evaluated in these sets of samples. Each sample was manually packed in metallic rings (approximately 100 cm^3, with an internal height and diameter of approximately 5 cm). To obtain clods for evaluating tensile strength and material for rheometric tests, we assembled larger specimens (volume of

approximately 330 cm^3, height and diameter of approximately 7.5 cm), where samples were packed with the aid of a hydraulic press. The initial bulk density of each test specimen was defined as the bulk density of the horizon where soil material was collected (1550 kg m^{-3}).

In a study on horizons with cohesive character, Vieira et al. (2012) found that samples packed with air-dried fine earth, when subjected to wetting and drying cycles, tend to exhibit strong cohesion when dry. Therefore, all experimental units were subjected to ten cycles of wetting and drying to allow for structural changes and the manifestation of cohesive character. One cycle was conducted per week, from August 23, 2021, to November 1, 2021, totaling ten weeks. The ten-week interval allowed biochar doses to promote changes in the structure detectable by the used soil physical quality indicators. Always at 2 PM, on Monday, the samples were placed on sponges saturated with distilled water to moisten by capillarity. After that, every Wednesday at 2 PM, the samples were removed from the sponges and left to air-dry in plastic trays, where the samples remained until the following Monday. Thus, the cycle consists of two days of wetting and five days of air drying. The average, minimum, and maximum temperatures in the laboratory where the study was conducted were 28.8, 26.6, and 30.8 ºC, respectively.

2.3. Analyzed attributes

2.3.1. Silicon adsorption capacity

At the end of the wetting-drying cycles, the test specimens were removed from the aluminum rings and disaggregated manually. The material obtained was used to perform silicon adsorption capacity tests for the soil + biochar mixture, at the respective biochar doses. For this purpose, in triplicates, 5 g of the material was added to 50 mL Falcon tubes along with 25 mL of a solution containing 10 ppm of Si (1:5 w/v), using Na_4SiO_4 as the Si source due to its good water solubility. This mixture was stirred for 24 hours on a horizontal mechanical shaker, centrifuged for 5 minutes at 5000 rpm (3214 G), and, finally, the supernatant was collected to determine the remaining Si in solution.

Quantification of remaining Si after equilibrium was carried out by UV–VIS spectroscopy at a wavelength of 660 nm, following the molybdenum blue colorimetric method as described by Kilmer (1965). The method is based on the formation of a yellow silico-molybdic complex that, after the addition of ascorbic acid, turns blue, allowing the Si quantification even at small concentrations. The Si adsorption capacity was calculated using Eq. (1):

$$q_e = \frac{(C_i - C_r) \times V}{m} \tag{1}$$

where q_e is the Si adsorption capacity (mg g^{-1}), C_i is the initial concentration of the solution (mg L^{-1}), C_r is the remaining concentration after equilibrium (mg L^{-1}), V is the supernatant volume (L), and m is the mass of adsorbent (g).

2.3.2. Soil bulk density and porosity

Soil bulk density was determined by considering the soil volume in the metallic rings after cycles of wetting and drying. Using the cross-sectional area of the ring and the height of each sample, volume was calculated. The mass of the particles, on the other hand, was obtained after drying the samples in an oven (105°C, until constant mass). Then, bulk density was calculated using Eq. (2) (Blake and Hartge, 1986a),

$$\rho_s = \frac{M_p}{V_s} \tag{2}$$

where ρ_s is the bulk density (kg m^{-3}); M_p is the mass of particles (kg), and V_s is the soil volume (m^3).

Total porosity was obtained using the data of soil and particle densities, according to Eq. (3),

$$\alpha = \left(1 - \frac{\rho_s}{\rho_p}\right) \tag{3}$$

where α is the total porosity (m^3 m^{-3}), and ρ_p and ρ_s are the particle density and bulk density (kg m^{-3}), respectively. Soil particle density was obtained for each treatment using the volumetric flask method, which involves determining the volume of alcohol needed to fill a 50 mL volumetric flask containing 20 g of the material to be analyzed. The volume of particles is equal to the difference between the flask volume and the volume of used alcohol (Blake and Hartge, 1986b).

Microporosity was determined by applying a pressure of 6 kPa on a tension table to empty macropores (Klute, 1986). Macroporosity was calculated as the difference between total porosity and microporosity.

2.3.3. Penetration resistance and tensile strength

Penetration resistance was determined with test specimens with moisture equilibrated to −33 kPa tension, commonly associated with field capacity (Assouline and Or, 2014). We used a static cone penetrometer with a linear actuator system operating at a speed of 1 cm min^{-1}, a load cell of 2000 kPa, and a cone with a base diameter of 0.4 cm, an angle of 60°, and an area of 12.566 mm^2. The penetrometer used is connected to a microcomputer for data acquisition, as described by Tormena et al. (1998), recording one reading per second. Three equidistant readings were taken for each experimental unit.

To determine tensile strength, the test specimens with a volume of approximately 330 cm^3 (height and diameter of 7.5 cm) were moistened by capillarity and subsequently disintegrated into clods with diameters ranging from 19 to 25 mm. The clods were air-dried before the tests. Tensile strength tests were conducted using a dynamometer with an electronic linear actuator at a constant speed of 0.08 mm s^{-1} (Tormena et al., 2008). Five clods from each experimental unit were analyzed, so that the tensile strength for the respective repetition corresponded to the mean value of the five clods. Thus, 25 clods per treatment were tested. Before evaluation, the mass of each clod was determined using an analytical scale. The arithmetic mean of the tensile strength of the five clods was used to define the value of the respective replication.

Each clod was individually placed in the most stable position between two metal plates: one fixed to the base of the equipment and the other mobile and connected to the load cell of the electronic linear actuator (capacity of 2000 kPa). The applied load value at clod rupture was stored by an electronic data acquisition system. After each rupture procedure, the mass of a portion of each clod was measured, and then the material was oven-dried (105°C for 48 hours) for moisture calculation.

Tensile strength (TS) was evaluated, following Dexter and Kroesbergen (1985), by Eq. (4),

$$TS = \frac{0,576P}{D^2 10^3} \tag{4}$$

where TS is the tensile strength of the clod (kPa); 0.576 is the proportionality constant relating the applied compressive stress to the tensile stress generated within the clod; P is the applied force (N); and D is the effective diameter of the clod (m), calculated with Eq. (5) (Watts and Dexter, 1998),

$$D = Dm\left(\frac{M}{M_0}\right)^{0.333} \tag{5}$$

where D is the effective diameter of the clod (m); Dm is the mean diameter of the clods (m), obtained by averaging the sizes of the sieve openings; M is the mass of the clod when dried at 105°C (g); and M_0 is the mean mass of the clods when dried at 105°C (g).

2.3.4. Rheometric analyses

For the rheometric tests, samples with a bulk density equal to that of

the soil under study (1550 kg m^{-3}) were prepared using homogenized material from the test specimens previously undergone cycles of wetting and drying. Homogenized material was chosen because of the small final sample volume (only a few cm^3), and the assessment is very sensitive to structural heterogeneities such as cracks and fissures.

Soil bulk density is one of the factors that affect the rheological behavior of the soil (Holthusen et al., 2020b), so all the samples were packed with the same density. Furthermore, it should be considered that soil structure has little effect on the rheological properties, as the sample volume is small and the main acting forces depend on the electrostatic interactions between the particles and the presence of binding agents (Markgraf et al., 2006). On the other hand, Holthusen et al. (2019), found quite different results for the same soil material with preserved structure and after homogenization. Nonetheless, most soil rheological studies are conducted with deformed soil samples, from the earliest oscillatory tests applied to agricultural soils (Ghezzehei and Or, 2001; Holthusen et al., 2010; Markgraf et al., 2006; Or and Ghezzehei, 2002) to recent ones (Batista et al., 2022; Batistaão et al., 2020a, 2020b; Holthusen et al., 2019; Sobucki et al., 2022).

Before the rheological tests, the samples were saturated with distilled water in Petri dishes and then equilibrated on tension tables to a matric potential of −10 kPa (Sobucki et al., 2022). Subsequently, the amplitude sweep test (AST) was performed using a modular compact rheometer (MCR 102, Anton Paar, Germany), equipped with a measurement system with rough parallel plates of 25 mm (upper plate) and 50 mm in diameter (lower plate). Immediately before the test, the samples were horizontally cut at a height of approximately 4.5 mm using a nylon thread, and vertically using a 25 mm diameter ring. Thus, the diameter of the sample was adjusted to match the diameter of the upper plate of the equipment. The temperature of the lower plate was kept constant at 20°C; the gap distance between the plates was 4.0 mm; the waiting time before the test was 30 seconds; the amplitude of deformation varied from 0.0001% to 100%; the angular frequency was 0.5 Hz; the number of measured points was 30; and the average test duration was 12 minutes. In addition, the moisture reduction during the test did not exceed 10% in any evaluation.

In oscillatory tests, the shear stress (τ, Pa) results from the force required to generate strain (γ, %) along the shear surface. The strain (γ, %) was calculated using Eq. (6), while the shear stress (τ, Pa) was calculated using Eq. (7) (Holthusen et al., 2010; Mezger, 2020):

$$\gamma = \frac{S}{h}100 \tag{6}$$

$$\tau = \frac{2M}{\pi r^3} \tag{7}$$

where γ is the strain (%); s is the deflection distance (m); h is the distance between the plates (m); τ is the shear stress (Pa); M is the torque required for deformation (N); and r is the radius of the upper plate (m).

To quantify the rheological properties of the soil through oscillatory tests, some parameters of classical mechanics are modified (Pértile et al., 2018, 2016). The shear modulus (G), derived from Hooke's law, must be modified for the condition of oscillatory stress, giving rise to a complex shear modulus (G*, Pa), as in Eq. (8),

$$G^* = \frac{\tau_A}{\gamma_A} \tag{8}$$

where G^* is the complex shear modulus (Pa); τ_A is the amplitude of shear stress τ (Pa); and γ_A is the amplitude of strain γ (%).

The complex shear modulus (G*, Pa) was divided into a storage modulus (G', Pa) (Eq. (9)) and a loss modulus (G'', Pa) (Eq. (10)). The storage modulus (G′, Pa) represents the elastic component of a material and relates to the fraction of energy stored and later released, while the loss modulus (G'', Pa) represents the viscous component of a material and relates to an imaginary fraction of energy that is permanently lost during flow (Mezger, 2020).

$$G' = \frac{\tau_A}{\gamma_A}\cos\delta \tag{9}$$

$$G'' = \frac{\tau_A}{\gamma_A}\text{sen}\delta \tag{10}$$

where G' is the viscoelastic storage modulus (Pa); G'' is the loss modulus (Pa); τ_A is the amplitude of shear stress τ (Pa); γ_A is the amplitude of strain γ (%); and δ is the phase shift angle obtained by the displacement of the response curve τ relative to the controlled γ curve. For viscoelastic substances like soil, $0 < \delta < 90°$.

The ratio of G'' to G′ results in the tangent of δ (Eq. (10)), called the "loss factor," as it relates to the amount of energy lost from the system with deformation. When $\delta < 1$ ($G' > G''$), the elastic component predominates, and when $\delta > 1$ ($G' < G''$), the viscous component is predominant (Markgraf et al., 2006):

$$\tan\delta = \frac{G''}{G'} \tag{10}$$

where tanδ is the loss factor (-); G'' is the loss modulus (Pa); and G' is the viscoelastic storage modulus (Pa).

To obtain final rheological properties in an amplitude sweep test, the values of G', G'', tan δ, and τ are graphically represented as functions of γ, as illustrated in Fig. 2. With the curves of G′ and G" as a function of γ (Fig. 2A), the linear viscoelastic range (LVE) was determined. This range is defined as the region of the curve where G′ and G" are constant and a limit strain value (γLVE, %) has not been reached, indicating irreversible changes in the sample's structure (Holthusen et al., 2010; Mezger, 2020). Considering the intersection of the G' and G" curves as a function of γ (Fig. 2A), we calculated the "yield point" (YP), where tan δ = 1 and G' = G" (G'G" YP), meaning the viscous and plastic components are equal. This value occurs in the nonlinear viscoelastic range and defines the critical deformation (γYP, %) at which the viscous component predominates, and the sample irreversibly flows. The associated stress (τYP, Pa) at γYP was also obtained (Holthusen et al., 2019, 2010; Markgraf et al., 2006; Mezger, 2020; Pértile et al., 2018, 2016).

Also based on the G′ and G" curves as a function of γ (Fig. 2A), the integral z (Fig. 2A) and the maximum shear stress (τmax, Pa) were determined (Fig. 2B). The integral z is calculated as the area defined, at the lower limit, by the tanδ curve and, at the upper limit, by the line parallel to the x-axis at the level of YP (tan δ = 1). The higher the integral z value, the greater the proportion of elastic deformation and the greater the soil stiffness. The τmax value is obtained by observing the highest τ (Pa) value in each test. The τmax value indicates the maximum shear stress supported by the soil before the main friction is overcome (Holthusen et al., 2010; Markgraf, 2011; Markgraf et al., 2006; Mezger, 2020; Pértile et al., 2018). The rheological properties were calculated using Rheoplus/32 v 3.62 software (Anton Paar, Germany).

2.4. Statistical analysis

The normality of the data was assessed using the Shapiro-Wilk, Kolmogorov-Smirnov, Cramer-von Mises, and Anderson-Darling tests ($P < 0.05$). In cases where normality was not confirmed, data transformation was performed using the Box and Cox (1964) procedure, which seeks to find an optimal power (λ) such that the transformed data assume a distribution as close as possible to normal.

Analysis of variance (ANOVA) was performed using the F-test, and mean comparisons were conducted using the Tukey test ($P < 0.05$). Regression and correlation analyses were carried out between the evaluated attributes and the biochar doses, considering linear ($y = ax + b$) and quadratic models ($y = ax^2 + bx + c$). The significance of the linear regression coefficient (a) and the dominant coefficient of the polynomial (a) was tested. The model that provided the best fit (r^2) and was

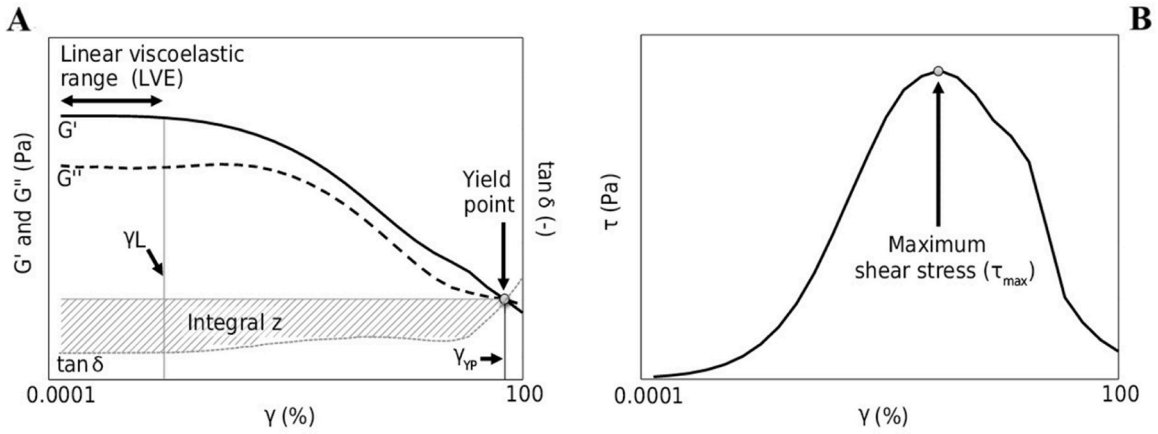

Fig. 2. Illustration of rheological properties obtained in an amplitude sweep test (AST). Viscoelastic storage modulus (G′), loss modulus (G″), and loss factor (tan δ) as functions of deformation (γ) (Logarithmic scale) (A). Shear stress (τ) as a function of strain (γ) (B). Source: Pértile et al. (2016).

statistically significant was chosen. Principal component analysis (PCA) was conducted to characterize the treatments, and cluster analysis was performed to group treatments with higher similarity. All analyses were conducted using the SAS® OnDemand for Academics platform.

3. Results and discussion

3.1. Silicon adsorption capacity

From the results of silicon removal from the solution (Na_4SiO_4 10 ppm), there was a removal of 37.5, 37.4, 37.2, 40.3, and 43.2% for treatments B0, B5, B10, B20, and B40, respectively. Silicon adsorption capacity (q_e) was affected by the treatments (Fig. 3A), with an increase in q_e as the proportion of biochar increased in the soil + biochar substrate (Fig. 3B). This increase was noticeable starting from the dose of 20 Mg ha^{-1}, with q_e reaching the maximum value (0.0220 mg g^{-1}) at the 40 Mg ha^{-1} dose (Fig. 3A). Considering the 40 Mg ha^{-1} dose and the studied horizon (bulk density of 1550 kg m^{-3} and thickness of 0.49 m), this result implies the capacity of adsorbing an additional 11.2 kg of Si per hectare compared to the control treatment.

At the lowest doses (5 and 10 Mg ha^{-1}), the q_e remained statistically unchanged relative to the control treatment, which suggests that high doses of the conditioner (> 20 Mg ha^{-1}) may be necessary to achieve significant improvement of the silicon adsorption capacity. Additionally, the dose of 20 Mg ha^{-1} appears to be a threshold from which increasing the biochar dose results in a proportional increase in Si adsorption capacity due to the greater proportion of the adsorbent in the system. Wang et al. (2018), in a study evaluating the dissolution kinetics of silicon by adding biochars to the soil (pyrolyzed biomass: rice husk, rice straw, sawdust, and orange peel; application rate: 2.5% w/w), state that once incorporated into the soil, the conditioner can adsorb silicon, presumably in its porous structure, through a process of physical adsorption – which makes it a reservoir (sink) for the element. This effect is more pronounced for biochar derived from materials with low silicon content, especially those from non-accumulator plant species (Wang et al., 2019), such as cashew – the plant whose residues were used to obtain the biochar that we utilized. Therefore, other biomass sources can be used when aiming to obtain biochar with the capacity to adsorb silicon, taking care to use plants that do not accumulate the element to favor the adsorption over its release.

Horizons with cohesive character result from densification because of reversible polymerization and precipitation of low crystalline siliceous and silico-aluminous compounds (Araújo Filho et al., 2001). Therefore, it can be inferred that the biochar derived from cashew bagasse residues has the potential to adsorb silicon, preventing its precipitation and, consequently, acting as a mitigator of the already established cohesion; likely, interrupting the process of formation of horizons with cohesive character.

3.2. Bulk density and porosity

There was no significant change in bulk density from 0 to 20 Mg ha^{-1} doses; however, at 40 Mg ha^{-1} the bulk density was significantly reduced, approximately 0.8% lower concerning the control treatment. It is important to mention that all samples, regardless of treatment, were prepared with the same initial bulk density. Therefore, the reduction in bulk density after the experimental period occurred due to modifications in the soil structure provided by the added biochar. The application of

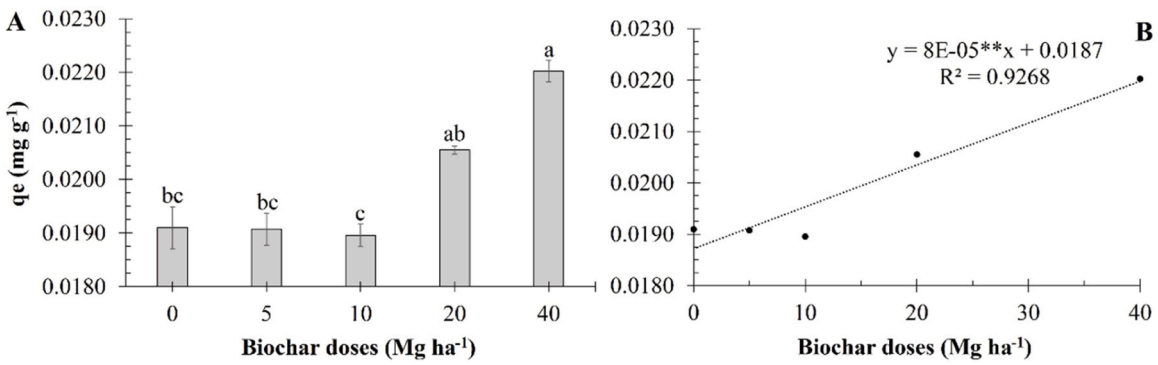

Fig. 3. Mean values of silicon adsorption capacity (q_e) as a function of biochar doses (A). Regression between q_e and biochar doses (B). Means followed by the same letter do not differ according to the Tukey test ($P < 0.05$). Bars represent the standard error of the mean. **Significant regression coefficient ($P < 0.01$).

biochar promotes the aggregation of soil particles, improving soil porosity, which implies an increase in pore volume and a reduction in bulk density (Nascimento et al., 2023). These processes occur because biochar particles can interact with cations and mineral particles and reduce the net balance of repulsive forces in the soil, favoring the aggregation process (Glaser et al., 2002; Hu et al., 2021; Ibrahim et al., 2013). Horizons with cohesive character have a high bulk density (between 1500 and 1800 kg m^{-3}) (Araújo Filho et al., 2001; Ribeiro, 2001), and often exhibit weak structural organization (Lima Neto et al., 2009). Therefore, strategies that promote aggregation – increasing porosity and reducing bulk density – are crucial to providing a physical soil environment more favorable for plant development.

Soil bulk density is usually greater than the density of various types of biochar. Thus, in the field, the mixture of a material with low density (biochar) with another of high density (soil) results in a reduction in the mass/volume ratio of the mixture, i.e., in bulk density after conditioner

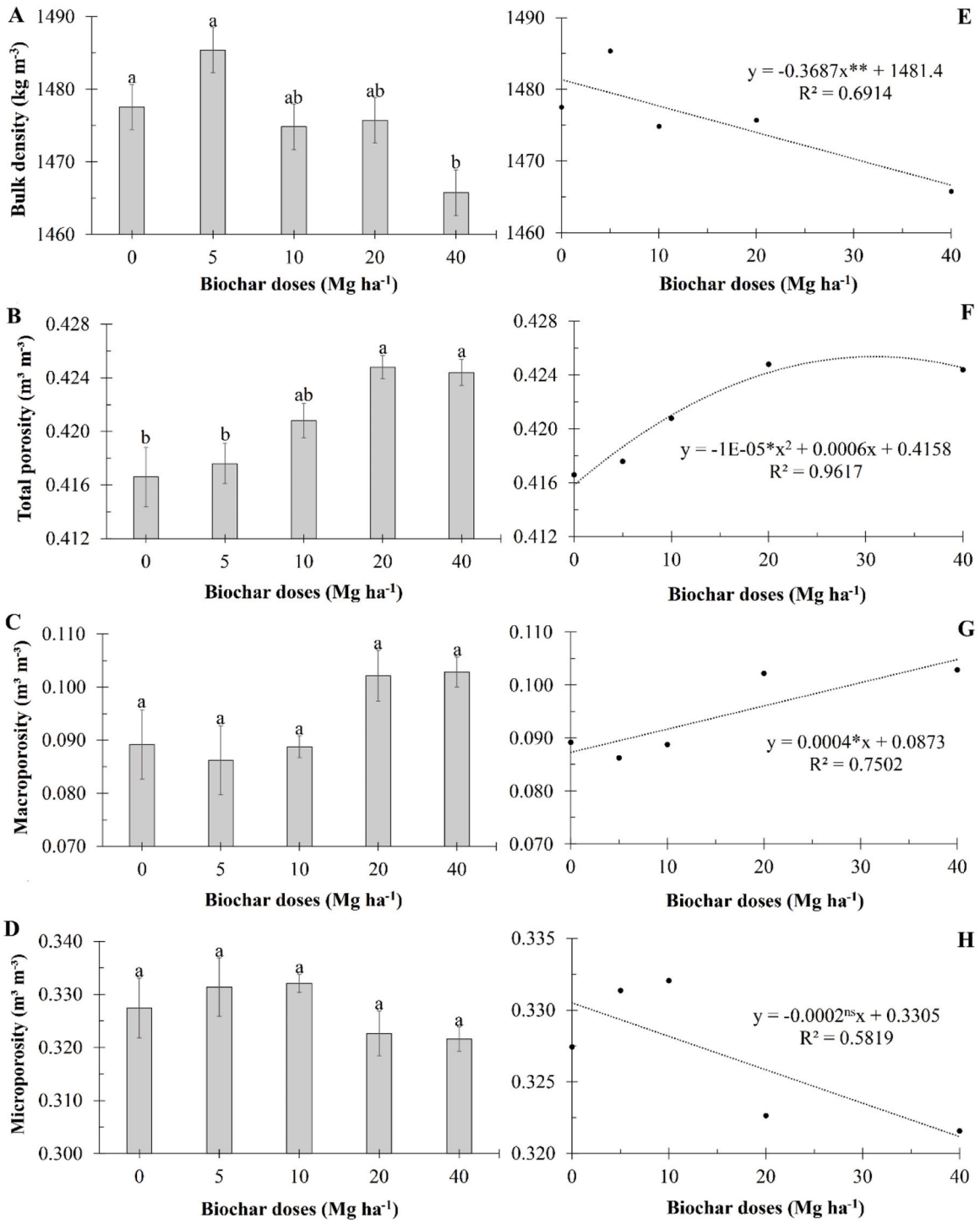

Fig. 4. Mean values of Bulk density (A); Total porosity (B); Macroporosity (C); and Microporosity (D) as a function of biochar doses. Regression between Bulk density (E); Total porosity (F); Macroporosity (G); and Microporosity (H) and biochar doses. Means followed by the same letter do not differ according to the Tukey test ($P < 0.05$). Bars represent the standard error of the mean. **Significant regression coefficient ($P < 0.01$). *Significant regression coefficient ($P < 0.05$). ^{ns}Not significant regression coefficient.

incorporation. This effect becomes more pronounced with higher application rates, and greater differences between bulk density and biochar density (Blanco-Canqui, 2017). Bulk density is a key indicator related to other soil physical properties, such as total porosity and mechanical resistance to root penetration (Al-Shammary et al., 2018; Keller and Håkansson, 2010). Therefore, as expected, the reduction in density through the application of biochar improved other evaluated physical soil quality indicators, as discussed below.

Total porosity exhibited a parabolic relationship with biochar dose (Fig. 4F). The maximum value of the quadratic equation corresponds to a dose of 30 Mg ha^{-1} and a total porosity of 0.4248 m^3 m^{-3} (x and y coordinates of the vertex of the parabola, respectively). In this way, a maximum plateau of total porosity was reached given the mixture of soil with biochar, so that the addition of biochar, even at high doses (> 50 Mg ha^{-1}) would probably not result in increases in the variable.

Doses of 20 and 40 Mg ha^{-1} showed the highest total porosities (0.4248 and 0.4244 m^3 m^{-3}, respectively), differing from doses of 0, 5, and 10 Mg ha^{-1} (Fig. 4B). Voids between particles and aggregates form a complex network of pores of various sizes (Ambus et al., 2023; Hao et al., 2008), whose functionality is crucial for plant development. Aggregation provided by the interaction between biochar particles and soil particles can result in the formation of new pores, leading to an increase in total porosity.

Macroporosity did not differ statistically according to the Tukey test (P <0.05) (Fig. 4C), although there was a linear response of macroporosity to the biochar doses (Fig. 4G). The regression analysis demonstrates the effects of treatments on the soil. Only the 20 and 40 Mg ha^{-1} doses showed macroporosity greater than 0.1 m^3 m^{-3} (10%), which corresponds to the minimum aeration porosity required for the proper development of most crops (Grable and Siemer, 1968).

Studying horizons with and without cohesive character in the state of Ceará, Brazil, Mota et al. (2018), concluded that cohesive horizons have lower macroporosity, which results in restrictions to water and air flow and hinders plant growth. Thus, biochar application emerges as an alternative to improve permeability in cohesive horizons, given that air (Holthusen et al., 2018a; Mentges et al., 2016; Reichert et al., 2022) and water flow (Reichert et al., 2016b, 2009) predominantly occur in macropores. Another factor to consider was the ten weeks of the experimental period, coinciding with soil wetting and drying cycles. Therefore, it is suggested that new studies be conducted with longer periods to verify if the changes imposed by the conditioner can be even more pronounced.

Microporosity was not affected by the application of biochar (Fig. 4D), and there was no significant correlation between these variables (Fig. 4H). This behavior corroborates the statement that the increase in total porosity due to the conditioner application was provided by the increase in macroporosity, not by a potential increase in microporosity, which remained statistically constant. However, the last two values of microporosity are slightly lower than at the control and at biochar doses < 10 Mg ha^{-1}. Possibly, doses > 40 Mg ha^{-1} or intermediate (15, 25, 30 Mg ha^{-1}) might result in a significant trend of decreasing microporosity with higher biochar dosage.

3.3. Penetration resistance and tensile strength

Penetration resistance (PR), measured at field capacity (Ψm = −33 kPa), reduced with increasing biochar dose, with the vertex coordinates of the quadratic function corresponding to a PR of 1.27 MPa and a dose of 24.1 Mg ha^{-1} (Fig. 5A). The PR reduction was significant from the dose of 10 Mg ha^{-1}, reaching the lowest values at doses of 10, 20, and 40 Mg ha^{-1} (reduction of 13.3, 16.2, and 16.1%, respectively) (Fig. 5C). The reduction of PR is in line with the increased Si adsorption capacity (Fig. 6), as the latter is supposed to reduce the cohesion and the mechanical resistance.

There was a correlation of 43.9% between PR and bulk density, following the Busscher et al. (1997) model. Thus, a crucial factor in reducing PR was the reduction in bulk density provided by the conditioner (Fig. 4A and E). According to Blanco-Canqui (2017), the effects of

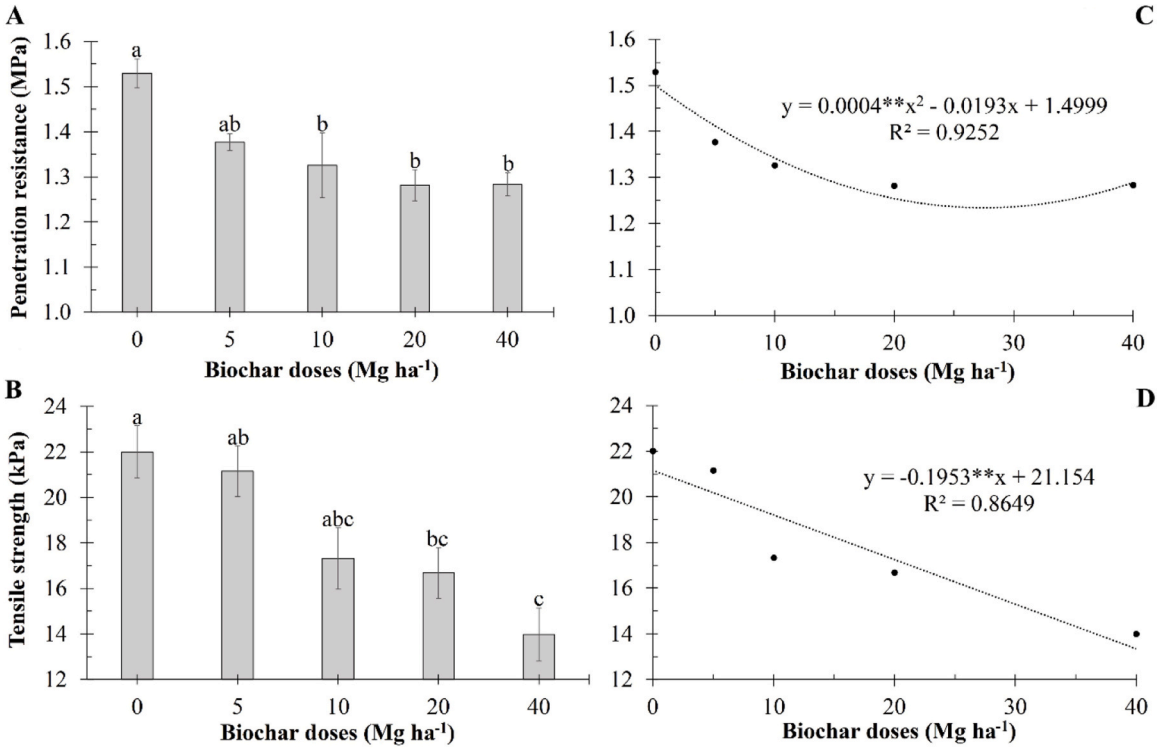

Fig. 5. Mean values of Penetration resistance (Ψm = −33 kPa) (A); and Tensile strength (B) as a function of biochar doses. Regression between Penetration resistance (C); and Tensile strength (D) and biochar doses. Means followed by the same letter do not differ according to the Tukey test (P < 0.05). Bars represent the standard error of the mean. **Significant regression coefficient (P < 0.01).

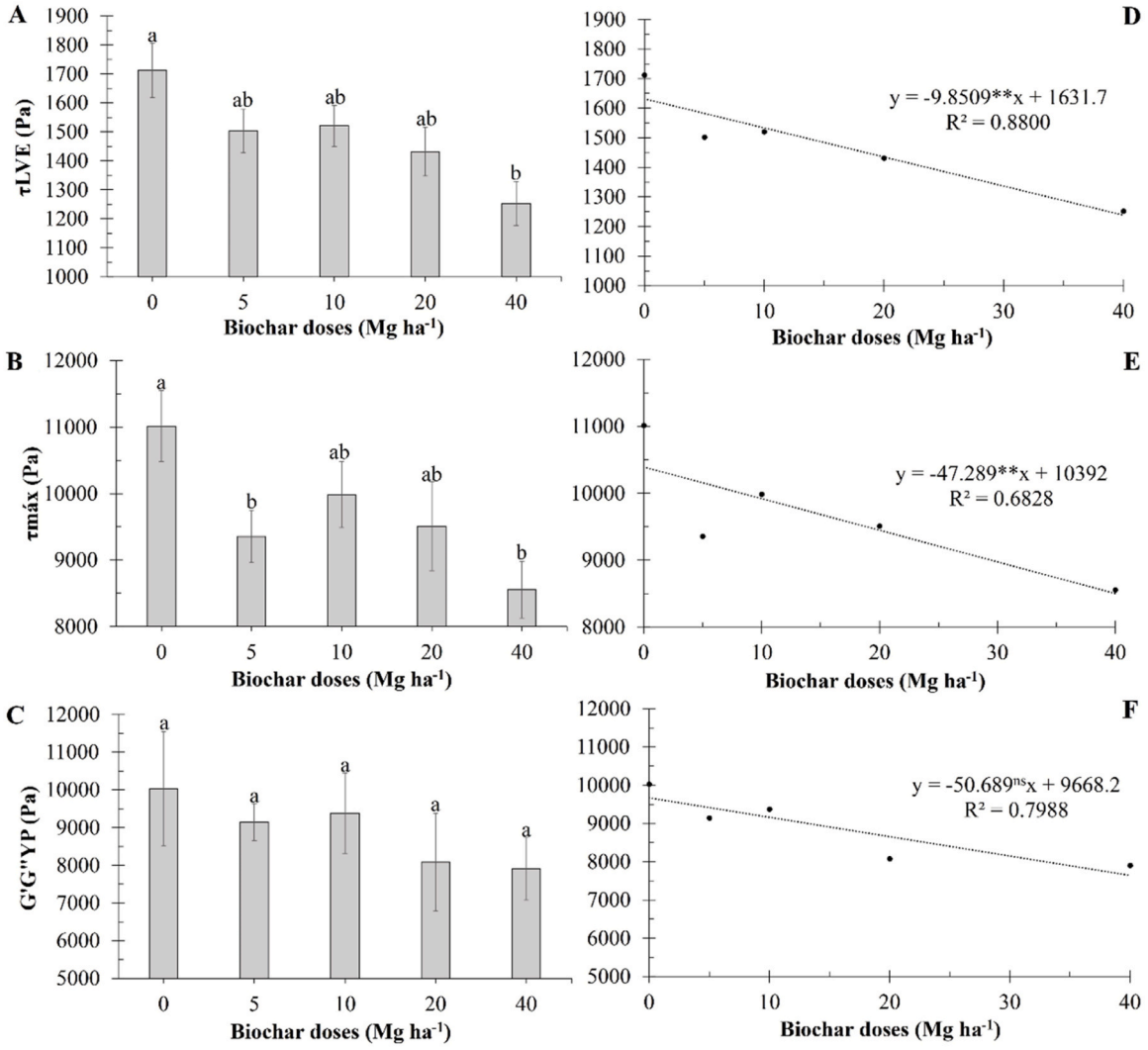

Fig. 6. Mean values of properties related to shear strength: Stress at the end of the linear viscoelastic range (τLVE) (A); Maximum shear stress (τmax) (B); and Storage and loss modulus at the yield point (G'G" YP) (C) as a function of biochar doses. Regression between τLVE (D); τmax (E); and G'G" YP (F) and biochar doses. Means followed by the same letter do not differ according to the Tukey test ($P < 0.05$). Bars represent the standard error of the mean. **Significant regression coefficient ($P < 0.01$); ^{ns}Not significant regression coefficient.

biochar application on PR may not be significant depending on the biochar dose and residence time in soil, often requiring high application rates and enough residence time for a noticeable change in the attribute. However, considering the scale of this experiment, the type of biochar, the experimental time, and the tested doses, there was a noticeable reduction in PR averages. The lower PR values associated with doses of 10, 20, and 40 Mg ha^{-1} require less mechanical effort and energy by the root system of plants growing in such cohesive soil.

All PR values, including the control treatment, were below 2 MPa – the critical PR threshold beyond which there is a physical restriction to the root growth of most cultivated crops (Cortez et al., 2018; Silva et al., 1994; Tormena et al., 1998). When moist, horizons with cohesive character exhibit a consistency ranging from friable to firm (Santos et al., 2018) which may result in lower PR values under dry soil conditions (maximum cohesion). However. the lower PR values were associated with biochar application.

Tensile strength (TS) reduced with increasing biochar dose (Fig. 5D), with a minimum value at the dose of 40 Mg ha^{-1} (13.98 kPa) (Fig. 5B). Horizons with cohesive character typically have higher TS values than non-cohesive horizons (Mota et al., 2021). Biochar application was effective in reducing TS and, therefore, the cohesion of this horizon, since the conditioner promotes Si adsorption (Fig. 3), reducing the precipitation of the element and acting as a mitigator of the existing cohesion.

The importance of organic materials in cohesion, shear strength, and load transmission within the soil has already been demonstrated for non-cohesive compactable soils, whether in the form of organic matter within the soil matrix (Braida et al., 2011, 2010, 2008, 2007; Holthusen et al., 2020a; Reichert et al., 2018), biochar (Alves et al., 2021; Awe et al., 2021), or as plant residue on the soil surface (Braida et al., 2006; Holthusen et al., 2018b; Reichert et al., 2016a). Biochar application reduced bulk density (Fig. 4A and E) because the conditioner promotes particle interaction and aggregation, increasing total porosity (Figs. 4B and F) and decreasing tensile strength (Ahmed and Raghavan, 2018; Sokołowska et al., 2020).

According to Zong et al. (2014), biochar application is a viable alternative for improving the physical quality of clayey soils, as is the case with the studied horizon (44.0% clay), resulting in a reduction in tensile strength with the incorporation of low-density, porous material. This material reduces the number of contact points between soil mineral particles, which in turn reduces shear stress and cohesion. The authors also claim that this reduction in mechanical resistance implies a decrease in energy consumption during soil cultivation operations. This effect is beneficial in horizons with cohesive character since, when dry,

cohesion increases to the point of hindering soil preparation operations and plant development (Giarola and Silva, 2002).

The more pronounced effect observed at the highest dose (40 Mg ha^{-1}) suggests that high doses of the conditioner may be necessary to achieve significant reductions in soil tensile strength (Sokołowska et al., 2020). However, reduction in frequency and cost of soil tillage operations, such as subsoiling, that are often necessary in areas with soils with cohesive character (Corrêa et al., 2023) may offset the expenses associated with biochar application, even at high doses. Another positive aspect is the persistence of biochar in the soil (Nascimento et al., 2023). This can be an advantage in tropical or subtropical regions where the mineralization of organic matter is accelerated due to high temperatures.

3.4. Rheometric properties

The τLVE and τmax decreased with the application of biochar, without affecting G′G′′YP (Fig. 6). For the two shear stress variables, the effects of the conditioner application were significant starting from the dose of 5 Mg ha^{-1}, with the lowest values corresponding to the dose of 40 Mg ha^{-1}.

One of the factors related to the reduction in τLVE and τmax is the decrease in the number of contact points between soil mineral particles provided by the application of biochar, resulting in reduced friction, cohesion, and shear strength (Zong et al., 2014). Another possibility is the lubricating effect that occurs due to the formation of water films on the surface of biochar particles, reducing microstructural shear resistance which is naturally high in the horizons of cohesive soils (Sobucki et al., 2022).

Soil structure, at the microscale, depends on electrostatic interactions between particles and the presence of cementing agents (Markgraf et al., 2006). Therefore, we infer that the biochar, by favoring the adsorption of Si instead of its precipitation (Fig. 3), favored the reduction of cohesion, reflecting the reduction of microstructural shear strength, particularly in τLVE and τmax. As discussed before, soil penetration resistance and tensile strength (Fig. 5) were also sensitive to cohesion reduction provided by biochar addition.

Despite the tendency for G′G′′ YP to decrease with increasing biochar dose, the linear regression coefficient was not significant, and there was no significant difference between the means. However, in soil with biochar application, structure collapsed and flow occurred at lower stresses than in the control treatment, indicating lower resistance to applied stress (Alves et al., 2021).

Fig. 7 shows the mean values of properties related to soil viscoelasticity at the microstructural level as a function of biochar doses. There was a significant trend of γLVE reduction with increasing doses of

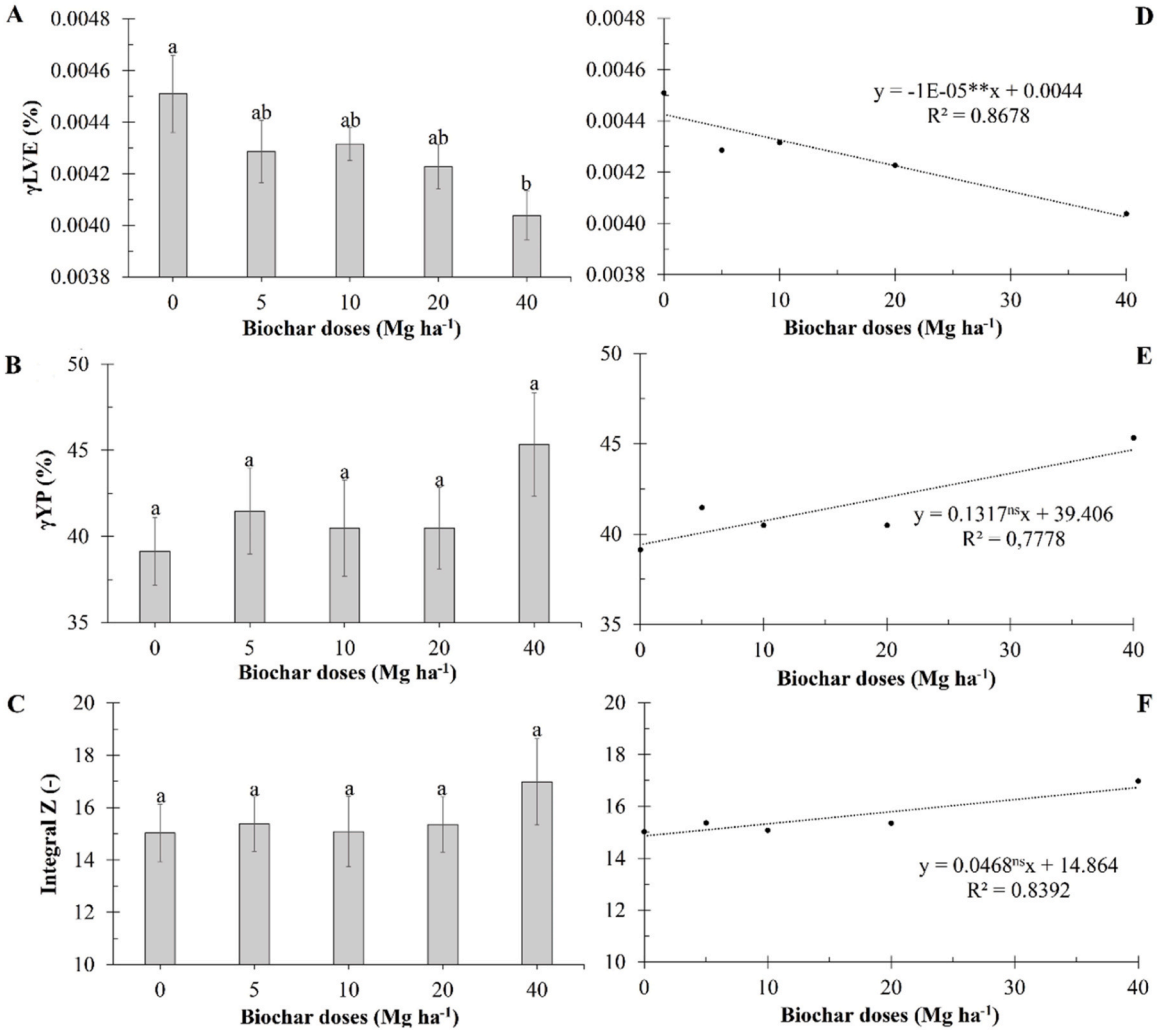

Fig. 7. Mean values of properties related to viscoelasticity: Deformation at the end of the linear viscoelastic range (γLVE) (A); Deformation at the yield point (γYP) (B); and Integral Z (C) as a function of biochar doses. Transformed variables (λ = −1.89, −0.72, and −0.81, respectively). Regression between γLVE (D), γYP (E), Integral Z (F), and biochar doses. Means followed by the same letter do not differ according to Tukey's test (P <0.05). The bars represent the standard error of the mean. **Significant regression coefficient (P <0.01); ^{ns}Not significant regression coefficient.

biochar (Fig. 7A). The effect of the conditioner application was significant, with the lowest value associated with the dose of 40 Mg ha^{-1} (Fig. 7D). Therefore, the strain value that signals irreversible changes in soil structure (γLVE) (Holthusen et al., 2010; Mezger, 2020) was reached earlier in soil with biochar application (the earlier the higher application), which can be interpreted as an indicator of lower microstructural stability.

The γYP (Fig. 7B) and Integral Z (Fig. 7C) were not affected by the studied treatments. The regressions between these variables and the respective doses of biochar were also not significant. When applying biochar obtained from the pyrolysis of rice and soybean straw (10 Mg ha^{-1}) to soil samples collected in the topsoil of a Typic Hapludult, Alves et al. (2021) also reported little or no modification in soil properties related to viscoelasticity after biochar in soil for 15, 30, 45, and 60 days, highlighting the needing for longer residence time of biochar for the detection of its effects on soil rheometric attributes. The authors emphasize that this was not expected since the increase in electrostatic interactions and specific surface area of the soil provided by the conditioner should result in changes in viscoelasticity, relating the findings to residence time and applied dose. In our study, a 70-day experimental period and a dose of 40 Mg ha^{-1} were sufficient to significantly change γLVE but not γYP and Integral Z, suggesting the need for evaluation at higher doses and longer residence periods of biochar in the soil.

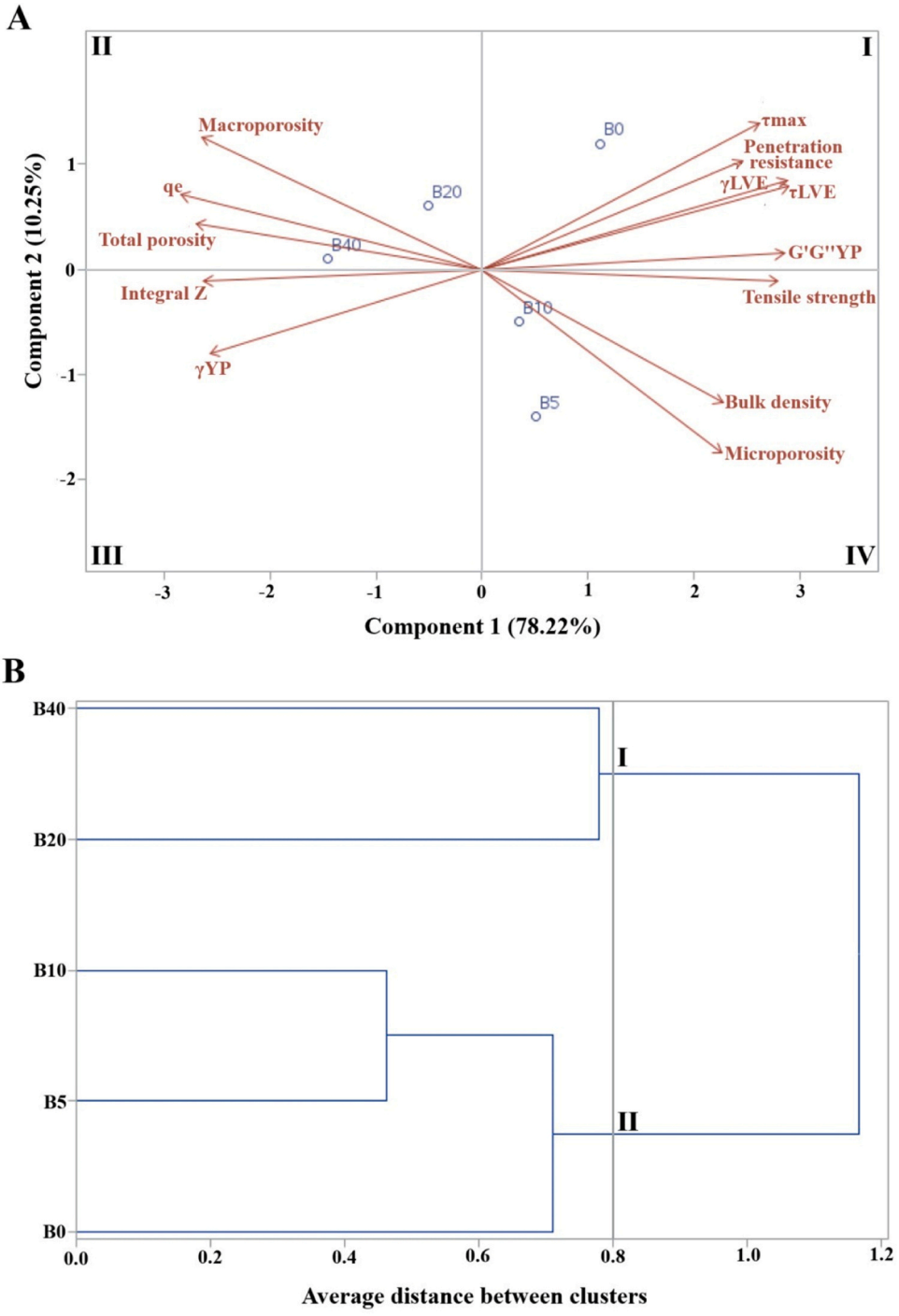

Fig. 8. Biplot graph, used to characterize the treatments (A); and Dendrogram, used to group treatments with higher similarity (B).

Improvement in physical quality and agronomic performance of soils and other substrates receiving biochar application results from the enhancement in microstructural conditions, as assessed in rheometry tests (Ajayi and Horn, 2016). In our study, the improvement provided by the conditioner was detectable through rheological properties, with particular emphasis on τLVE, τmax, and γLVE.

3.5. Multivariate analysis

In the principal component analysis (Fig. 8A), components 1 and 2 together explained 88.47% of the data variability. According to Jolliffe and Cadima (2016), it is common to select the number of components to explain at least 70% of the variance.

When analyzing quadrant I of the biplot graph (Fig. 8A), the control treatment (B0) is associated with a condition of greater microstructural stability and, consequently, higher cohesion, with values of τmax, τLVE, G'G" YP, and γLVE above the mean. Treatment B0 has penetration resistance above the mean, which is common in horizons with cohesive characteristics. The rheological properties τmáx, τLVE, G'G" YP, and γLVE high positive correlation with PR (83.38%, 87.39%, 86.74%, and 86.70%, respectively) and TS (73.69%, 88.35%, 84.24%, and 87.06%, respectively). These correlations show rheometry is an important tool in characterizing horizons with cohesive character, as it is sensitive to modifications imposed on soil structure by management strategies.

In quadrant II are treatments B20 and B40, associated with values of silicon adsorption capacity, total porosity, and macroporosity above the mean, as well as tensile strength, microporosity, and soil density below the mean. Thus, the application of biochar, especially at higher doses (20 and 40 Mg ha^{-1}), favored the flocculation of soil particles, which is the first stage of aggregate formation, resulting in reduced bulk density and increased total porosity and macroporosity.

The correlation matrix generated in the principal component analysis shows that tensile strength and silicon adsorption capacity had a strong negative correlation (-82.37%). Therefore, the lower TS and higher silicon adsorption capacity in treatments B20 and B40 confirm that biochar, by adsorbing silicon, leads to a decrease in tensile strength and, consequently, cohesion in horizons with cohesive character.

In quadrant IV, treatments B5 and B10 are associated with values of silicon adsorption capacity, total porosity, and macroporosity below average, as well as bulk density, tensile strength, and microporosity above average. Thus, the application of biochar at low doses is not sufficient to improve attributes related to the soil porous network and to promote silicon adsorption and reduced cohesion, with physical quality remaining closer to treatment B0 than treatments B20 and B40.

Fig. 8B shows the dendrogram resulting from the cluster analysis. When drawing a limit at a multivariate distance of 0.8, two distinct groups are formed: group I, consisting of treatments B20 and B40, where the effects of biochar application were more pronounced, resulting in reduced cohesion and mechanical resistance, and an increase in total porosity and macroporosity of the soil; and group II, consisting of treatments B0, B5, and B10, where the effects of biochar application are noticeable (B5 and B10), but not very pronounced, with physical quality remaining similar to the control treatment (B0). This information is important when choosing the dose of biochar to be applied in horizons with cohesive character, and it is recommended to use a dose between 20 and 40 Mg ha^{-1}.

4. Conclusions

The biochar produced from cashew residues has the potential to adsorb silicon, reducing the precipitation of silicate compounds that cause particle cementation. Thus, it acts to reduce the cohesion already established and attenuates the genetic process of temporary cementation in horizons with the cohesive character.

The application of biochar from cashew residues improves soil porosity and promotes silicon adsorption, thus reducing bulk density, cohesion, and mechanical resistance at meso and microstructural scales, leading to an improvement in the physical quality of soils with cohesive character. This could lead to a reduction in the frequency and cost of soil tillage operations, such as subsoiling, and may help offset the expenses associated with biochar application, even in substantial doses.

For soils with cohesive character, the benefits of applying cashew residues biochar are noticeable even at low doses between 5 and 10 Mg ha^{-1}. However, doses between 20 and 40 Mg ha^{-1} are more effective in improving soil physical quality, mitigating cohesion, and creating a soil physical environment more favorable for plant growth.

CRediT authorship contribution statement

José Miguel Reichert: Writing – review & editing, Writing – original draft, Supervision, Methodology, Investigation. **Ricardo Espíndola Romero:** Writing – review & editing, Writing – original draft, Methodology. **Jaedson Cláudio Anunciato Mota:** Writing – review & editing, Writing – original draft, Visualization, Validation, Supervision, Methodology, Investigation, Formal analysis, Data curation, Conceptualization. **Crisanto Dias Teixeira Filho:** Writing – review & editing, Writing – original draft, Methodology, Investigation, Formal analysis. **Alexandre dos Santos Queiroz:** Writing – review & editing, Writing – original draft, Methodology, Investigation, Formal analysis. **Arthur Prudêncio de Araujo Pereira:** Writing – review & editing, Writing – original draft, Methodology. **Ícaro Vasconcelos do Nascimento:** Writing – review & editing, Writing – original draft, Visualization, Methodology, Investigation, Formal analysis, Data curation, Conceptualization. **Francisca Gleiciane da Silva:** Writing – review & editing, Writing – original draft, Methodology. **Viviane Sobucki:** Writing – review & editing, Writing – original draft, Methodology, Investigation, Formal analysis. **Angélica da Silva Lopes:** Writing – review & editing, Writing – original draft, Methodology, Investigation, Formal analysis. **Helon Hébano de Freitas Sousa:** Writing – review & editing, Writing – original draft, Methodology. **Emanuela Barbosa dos Santos:** Writing – review & editing, Writing – original draft, Methodology, Investigation, Formal analysis. **Odair Pastor Ferreira:** Writing – review & editing, Writing – original draft, Methodology, Conceptualization. **Mirian Cristina Gomes Costa:** Writing – review & editing, Writing – original draft, Resources, Project administration, Methodology, Funding acquisition, Conceptualization. **Laís Gomes Fregolente:** Writing – review & editing, Writing – original draft, Methodology, Investigation, Formal analysis, Conceptualization. **Antônio Gomes Souza Filho:** Writing – review & editing, Writing – original draft, Resources, Project administration, Funding acquisition.

Declaration of Competing Interest

The authors declare that they have no known competing financial interests or personal relationships that could have appeared to influence the work reported in this paper.

Data availability

The data that has been used is confidential.

Acknowledgments

This study received support from the Agricultural Chief Scientist Program of the Government of the State of Ceará (Agreement 14/2022 SDE/ADECE/FUNCAP and Process 08126425/2020/FUNCAP) for the provision of innovation scholarships and financial support for conducting the research; and support from the Financial Agency for Studies and Projects (FINEP), grant number 0122017200. Í.V. Nascimento and A.S. Queiroz thank CAPES (Coordination for the Improvement of Higher Education Personnel) for the scholarship and research financial support (Code 001). A.S. Lopes and L.G. Fregolente appreciate the Ceará

Foundation to Support Scientific and Technological Development (FUNCAP) for the scholarship. J.C.A. Mota, M.C.G. Costa, A.P.A. Pereira, O.P. Ferreira and J.M. Reichert thank CNPq (National Council for Scientific and Technological Development) for the research grant (Processes: 303524/2022–7; 305907/2019–0; 305231/2023–5; 310821/2022–3 and 409205/2023–0; and 309079/2019–5) and the Low Carbon Agriculture INCT Project (Process: 406635/2022–6).

References

Ahmed, A.S.F., Raghavan, V., 2018. Influence of wood-derived biochar on the physico-mechanical and chemical characteristics of agricultural soils. Int. Agrophys 32, 1–10. https://doi.org/10.1515/intag-2016-0094.

Ajayi, A.E., Horn, R., 2016. Modification of chemical and hydrophysical properties of two texturally differentiated soils due to varying magnitudes of added biochar. Soil Tillage Res 164, 34–44. https://doi.org/10.1016/j.still.2016.01.011.

Al-Shammary, A.A.G., Kouzani, A.Z., Kaynak, A., Khoo, S.Y., Norton, M., Gates, W., 2018. Soil bulk density estimation methods: a review. Pedosphere 28, 581–596. https://doi.org/10.1016/S1002-0160(18)60034-7.

Alves, A.R., Holthusen, D., Reichert, J.M., Sarfaraz, Q., Silva, L.S., 2021. Biochar amendment effects on microstructure resistance of a sandy loam soil under oscillatory stress. J. Soil Sci. Plant Nutr. 21, 967–977. https://doi.org/10.1007/s42729-021-00414-2.

Araújo Filho, J.C., Carvalho, A., Silva, F.B.R., 2001. Investigações preliminares sobre a pedogênese de horizontes coesos em solos dos tabuleiros costeiros do Nordeste do Brasil. in: Workshop Coesão Em Solos Dos Tabuleiros Costeiros. Embrapa, Aracaju, pp. 123–142.

Assouline, S., Or, D., 2014. The concept of field capacity revisited: Defining intrinsic static and dynamic criteria for soil internal drainage dynamics. Water Resour. Res 50, 4787–4802. https://doi.org/10.1002/2014WR015475.

Awe, G.O., Reichert, J.M., Holthusen, D., Ambus, J.V., Faccio Carvalho, P.C., 2021. Characterization of microstructural stability of biochar-amended Planosol under conventional tillage for irrigated lowland rice ecosystem. Soil Tillage Res 212, 105051. https://doi.org/10.1016/j.still.2021.105051.

Batista, R.F., Reichert, J.M., Holthusen, D., Batistão, A.C., Daher, M., Schünemann, A.L., Fernandes Filho, E.I., Schaefer, C.E.G.R., Francelino, M.R., 2022. Freeze–thaw cycles affecting rheological properties of Antarctic soils. Geoderma 428, 116220. https://doi.org/10.1016/j.geoderma.2022.116220.

Batistão, A.C., Holthusen, D., Reichert, J.M., Santos, L.A.C., Campos, M.C.C., 2020b. Resilience and microstructural resistance of Archaeological Dark Earths with different soil organic carbon contents in Western Amazonia, Brazil. Geoderma 363, 114130. https://doi.org/10.1016/j.geoderma.2019.114130.

Batistão, A.C., Holthusen, D., Reichert, J.M., Portela, J.C., 2020a. Soil solution composition affects microstructure of tropical saline alluvial soils in semi-arid environment. Soil Tillage Res 203, 104662. https://doi.org/10.1016/j.still.2020.104662.

Blake, G.R., Hartge, K.H., 1986b. Particle Density. In: Klute, A. (Ed.), Methods of Soil Analysis: Part 1 Physical and Mineralogical Methods. Soil Science Society of America, Madison, pp. 377–382. https://doi.org/10.2136/sssabookser5.1.2ed.c14.

Blake, G.R., Hartge, K.H., 1986a. Bulk Density. In: Klute, A. (Ed.), Methods of Soil Analysis: Part 1 Physical and Mineralogical Methods. Soil Science Society of America, Madison, pp. 363–375. https://doi.org/10.2136/sssabookser5.1.2ed.c13.

Blanco-Canqui, H., 2017. Biochar and Soil Physical Properties. Soil Sci. Soc. Am. J. 81, 687–711. https://doi.org/10.2136/sssaj2017.01.0017.

Box, G.E.P., Cox, D.R., 1964. An Analysis of Transformations. J. R. Stat. Soc.: Ser. B (Methodol.) 26, 211–243. https://doi.org/10.1111/j.2517-6161.1964.tb00553.x.

Braida, J.A., Reichert, J.M., Veiga, M., Reinert, D.J., 2006. Resíduos vegetais na superfície e carbono orgânico do solo e suas relações com a densidade máxima obtida no ensaio proctor. Rev. Bras. Cienc. Solo 30, 605–614. https://doi.org/10.1590/S0100-06832006000400001.

Braida, J.A., Reichert, J.M., Reinert, D.J., Soares, J.M.D., 2007. Coesão e atrito interno associados aos teores de carbono orgânico e de água de um solo franco arenoso. Ciência Rural 37, 1646–1653. https://doi.org/10.1590/S0103-84782007000600022.

Braida, J.A., Reichert, J.M., Reinert, D.J., Sequinatto, L., 2008. Elasticidade do solo em função da umidade e do teor de carbono orgânico. Rev. Bras. Cienc. Solo 32, 477–485. https://doi.org/10.1590/S0100-06832008000200002.

Braida, J.A., Reichert, J.M., Reinert, D.J., Veiga, M. da, 2010. Teor de carbono orgânico e a susceptibilidade à compactação de um Nitossolo e um Argissolo. Rev. Bras. De. Eng. Agr. ícola e Ambient. 14, 131–139. https://doi.org/10.1590/S1415-43662010000200003.

Braida, J.A., Bayer, C., Albuquerque, J.A., Reichert, J.M., 2011. Matéria orgânica e seu efeito na física do solo. In: Klauberg Filho, O., Mafra, Á.L., Gatiboni, L.C. (Eds.), Tópicos Em Ciência Do Solo. Sociedade Brasileira de Ciência do Solo, Viçosa, pp. 221–278.

Busscher, W.J., Bauer, P.J., Camp, C.R., Sojka, R.E., 1997. Correction of cone index for soil water content differences in a coastal plain soil. Soil Tillage Res 43, 205–217. https://doi.org/10.1016/S0167-1987(97)00015-9.

Campos, M., Penn, C.J., Gonzalez, J.M., Alexandre Costa Crusciol, C., 2022. Effectiveness of deep lime placement and tillage systems on aluminum fractions and soil chemical attributes in sugarcane cultivation. Geoderma 407, 115545. https://doi.org/10.1016/j.geoderma.2021.115545.

Corrêa, M.M., de Araújo Filho, J.C., Schaefer, Carlos E.G.R., Ker, J.C., 2023. Soils of the Coastal Tablelands Under Atlantic Forest (Tabuleiros Costeiros). In: Schaefer, C.E.G. R. (Ed.), The Soils of Brazil. World Soils Book Series. Springer, Cham, pp. 221–238. https://doi.org/10.1007/978-3-031-19949-3_8.

Cortez, J.W., Cavassini, V.H., Motomiya, A.V.A., Orlando, R.C., Valente, I.Q.M., 2018. Spatialization of soil resistance to penetration for localized management by precision agriculture tools. Eng. Agr. ícola 38, 690–696. https://doi.org/10.1590/1809-4430-eng.agric.v38n5p690-696/2018.

Dexter, A.R., Kroesbergen, B., 1985. Methodology for determination of tensile strength of soil aggregates. J. Agric. Eng. Res. 31, 139–147. https://doi.org/10.1016/0021-8634(85)90066-6.

Doran, J.W., Parkin, T.B., 1994. Defining and Assessing Soil Quality. In: Doran, J.W., Colemam, D.C., Bezdicek, D.F., Stewart, B.A. (Eds.), Defining Soil Quality for a Sustainable Environment. Soil Science Society of America, Madison, pp. 1–21. https://doi.org/10.2136/sssaspecpub35.c1.

Elkhlifi, Z., Iftikhar, J., Sarraf, M., Ali, B., Saleem, M.H., Ibranshahib, I., Bispo, M.D., Meili, L., Ercisli, S., Torun Kayabasi, E., Alemzadeh Ansari, N., Hegedűsová, A., Chen, Z., 2023. Potential Role of Biochar on Capturing Soil Nutrients, Carbon Sequestration and Managing Environmental Challenges: A Review. Sustainability 15, 2527. https://doi.org/10.3390/su15032527.

Fregolente, L.G., Rodrigues, M.T., Oliveira, N.C., Araújo, B.S., Nascimento, Í.V., Souza Filho, A.G., Paula, A.J., Costa, M.C.G., Mota, J.C.A., Ferreira, O.P., 2023. Effects of chemical aging on carbonaceous materials: Stability of water-dispersible colloids and their influence on the aggregation of natural-soil colloid. Science of The Total Environment 903, 166835. https://doi.org/10.1016/j.scitotenv.2023.166835.

Ghezzehei, T.A., Or, D., 2001. Rheological Properties of Wet Soils and Clays under Steady and Oscillatory Stresses. Soil Sci. Soc. Am. J. 65, 624–637. https://doi.org/10.2136/sssaj2001.653624x.

Giarola, N.F.B., Silva, A.P. da, 2002. Conceitos sobre solos coesos e hardsetting. Sci. Agric. 59, 613–620. https://doi.org/10.1590/S0103-90162002000300030.

Giarola, N.F.B., Silva, A.P., Tormena, C., Souza, L.S., Ribeiro, L.P., 2001. Similaridades entre o caráter coeso dos solos e o comportamento hardsetting: estudo de caso. Rev. Bras. Cienc. Solo 25, 239–247. https://doi.org/10.1590/S0100-06832001000100026.

Glaser, B., Lehmann, J., Zech, W., 2002. Ameliorating physical and chemical properties of highly weathered soils in the tropics with charcoal - a review. Biol. Fertil. Soils 35, 219–230. https://doi.org/10.1007/s00374-002-0466-4.

Grable, A.R., Siemer, E.G., 1968. Effects of Bulk Density, Aggregate Size, and Soil Water Suction on Oxygen Diffusion, Redox Potentials, and Elongation of Corn Roots. Soil Sci. Soc. Am. J. 32, 180–186. https://doi.org/10.2136/sssaj1968.03615995003200020011x.

Hao, X., Ball, B.C., Culley, J.L.B., Carter, M.R., Parkin, G.W., 2008. Soil Density and Porosity. In: Carter, M.R., Gregorich, E.G. (Eds.), Soil Sampling and Methods of Analysis. CRC Press, Boca Raton, pp. 743–760.

Hodson, M.J., White, P.J., Mead, A., Broadley, M.R., 2005. Phylogenetic Variation in the Silicon Composition of Plants. Ann. Bot. 96, 1027–1046. https://doi.org/10.1093/aob/mci255.

Holthusen, D., Peth, S., Horn, R., 2010. Impact of potassium concentration and matric potential on soil stability derived from rheological parameters. Soil Tillage Res 111, 75–85. https://doi.org/10.1016/j.still.2010.08.002.

Holthusen, D., Jänicke, M., Peth, S., Horn, R., 2012b. Physical properties of a Luvisol for different long-term fertilization treatments: II. Microscale behavior and its relation to the mesoscale. J. Plant Nutr. Soil Sci. 175, 14–23. https://doi.org/10.1002/jpln.201100076.

Holthusen, D., Jänicke, M., Peth, S., Horn, R., 2012a. Physical properties of a Luvisol for different long-term fertilization treatments: I. Mesoscale capacity and intensity parameters. J. Plant Nutr. Soil Sci. 175, 4–13. https://doi.org/10.1002/jpln.201100075.

Holthusen, D., Brandt, A.A., Reichert, J.M., Horn, R., Fleige, H., Zink, A., 2018b. Soil functions and in situ stress distribution in subtropical soils as affected by land use, vehicle type, tire inflation pressure and plant residue removal. Soil Tillage Res 184, 78–92. https://doi.org/10.1016/j.still.2018.07.009.

Holthusen, D., Brandt, A.A., Reichert, J.M., Horn, R., 2018a. Soil porosity, permeability and static and dynamic strength parameters under native forest/grassland compared to no-tillage cropping. Soil Tillage Res 177, 113–124. https://doi.org/10.1016/j.still.2017.12.003.

Holthusen, D., Pértile, P., Reichert, J.M., Horn, R., 2019. Viscoelasticity and shear resistance at the microscale of naturally structured and homogenized subtropical soils under undefined and defined normal stress conditions. Soil Tillage Res 191, 282–293. https://doi.org/10.1016/j.still.2019.04.014.

Holthusen, D., Pértile, P., Awe, G.O., Reichert, J.M., 2020b. Soil density and oscillation frequency effects on viscoelasticity and shear resistance of subtropical Oxisols with varying clay content. Soil Tillage Res 203, 104677. https://doi.org/10.1016/j.still.2020.104677.

Holthusen, D., Batistão, A.C., Reichert, J.M., 2020a. Amplitude sweep tests to comprehensively characterize soil micromechanics: brittle and elastic interparticle bonds and their interference with major soil aggregation factors organic matter and water content. Rheol. Acta 59, 545–563. https://doi.org/10.1007/s00397-020-01219-3.

Hu, F., Xu, C., Ma, R., Tu, K., Yang, J., Zhao, S., Yang, M., Zhang, F., 2021. Biochar application driven change in soil internal forces improves aggregate stability: Based on a two-year field study. Geoderma 403, 115276. https://doi.org/10.1016/j.geoderma.2021.115276.

Ibrahim, H.M., Al-Wabel, M.I., Usman, A.R.A., Al-Omran, A., 2013. Effect of Conocarpus Biochar Application on the Hydraulic Properties of a Sandy Loam Soil. Soil Sci. 178, 165–173. https://doi.org/10.1097/SS.0b013e3182979eac.

IUSS Working Group WRB, 2022. World Reference Base for Soil Resources. International soil classification system for naming soils and creating legends for soil maps, 4th ed. Vienna, Austria.
Jolliffe, I.T., Cadima, J., 2016. Principal component analysis: a review and recent developments. Philos. Trans. R. Soc. A: Math., Phys. Eng. Sci. 374, 20150202. https://doi.org/10.1098/rsta.2015.0202.
Kannan, V., Rangarajan, V., Manjare, S.D., Pathak, P.V., 2021. Microbial Production of Value-added Products from Cashew Apples- an Economical Boost to Cashew Farmers. J. Pure Appl. Microbiol 15, 1816–1832. https://doi.org/10.22207/JPAM.15.4.71.
Karlen, D.L., Mausbach, M.J., Doran, J.W., Cline, R.G., Harris, R.F., Schuman, G.E., 1997. Soil Quality: A Concept, Definition, and Framework for Evaluation (A Guest Editorial). Soil Sci. Soc. Am. J. 61, 4–10. https://doi.org/10.2136/sssaj1997.03615995006100010001x.
Keller, T., Håkansson, I., 2010. Estimation of reference bulk density from soil particle size distribution and soil organic matter content. Geoderma 154, 398–406. https://doi.org/10.1016/j.geoderma.2009.11.013.
Kilmer, V.J., 1965. Silicon. In: Norman, A.G. (Ed.), Methods of Soil Analysis: Part 2 Chemical and Microbiological Properties. Soil Science Society of America, Madison, pp. 959–962. https://doi.org/10.2134/agronmonogr9.2.c13.
Klute, A., 1986. Water Retention: Laboratory Methods. In: Klute, Arnold (Ed.), Methods of Soil Analysis: Part 1 Physical and Mineralogical Methods. Soil Science Society of America, Madison, pp. 635–662. https://doi.org/10.2136/sssabookser5.1.2ed.c26.
Koppen, W., 1918. Klassifikation der klimate nach Temperatur, Niederschlag und Jahreslauf. Petermanns Geogr. Mitt. 64, 193–248.
Lal, R., 2016. Soil health and carbon management. Food Energy Secur 5, 212–222. https://doi.org/10.1002/fes3.96.
Li, S., Tasnady, D., 2023. Biochar for Soil Carbon Sequestration: Current Knowledge, Mechanisms, and Future Perspectives. C. (Basel) 9, 67. https://doi.org/10.3390/c9030067.
Lima Neto, J. de A., Ribeiro, M.R., Corrêa, M.M., Souza Júnior, V.S., Lima, J.F.W.F., Ferreira, R.F. de A. e L., 2009. Caracterização e gênese do caráter coeso em latossolos amarelos e argissolos dos tabuleiros costeiros do estado de Alagoas. Rev. Bras. Cienc. Solo 33, 1001–1011. https://doi.org/10.1590/S0100-06832009000400024.
Luo, L., Wang, J., Lv, J., Liu, Z., Sun, T., Yang, Y., Zhu, Y.-G., 2023. Carbon Sequestration Strategies in Soil Using Biochar: Advances, Challenges, and Opportunities. Environ. Sci. Technol. 57, 11357–11372. https://doi.org/10.1021/acs.est.3c02620.
Ma, J.F., Takahashi, E., 2002. Silicon-accumulating plants in the plant kingdom. in: Soil, Fertilizer, and Plant Silicon Research in Japan. Elsevier, Amsterdam, pp. 63–71. https://doi.org/10.1016/B978-044451166-9/50005-1.
Markgraf, W., 2011. Rheology in Soils. Encycl. Agrophysics. https://doi.org/10.1007/978-90-481-3585-1_133.
Markgraf, W., Horn, R., Peth, S., 2006. An approach to rheometry in soil mechanics—Structural changes in bentonite, clayey and silty soils. Soil Tillage Res 91, 1–14. https://doi.org/10.1016/j.still.2006.01.007.
Marques, E. da S., Mota, J.C.A., Lacerda, C.F., Silva, F.G., Romero, R.E., 2021. Gas exchange in maize as a function of aeration porosity in a cohesive soil. Rev. Ciência Agron. ômica 52. https://doi.org/10.5935/1806-6690.20210035.
Mentges, M.I., Reichert, J.M., Rodrigues, M.F., Awe, G.O., Mentges, L.R., 2016. Capacity and intensity soil aeration properties affected by granulometry, moisture, and structure in no-tillage soils. Geoderma 263, 47–59. https://doi.org/10.1016/j.geoderma.2015.08.042.
Mezger, T., 2020. The Rheology Handbook, 5th ed. Vincentz Network, Hannover. https://doi.org/10.1515/9783748603702.
Mota, J.C.A., Menezes, A.S., Nascimento, C.D.V., Alencar, T.L., Assis Júnior, R.N., Toma, R.S., Romero, R.E., Costa, M.C.G., Cooper, M., 2018. Pore shape, size distribution and orientation in Bt horizons of two Alfisols with and without cohesive character from Brazil. Geoderma Reg. 15, e00197 https://doi.org/10.1016/j.geodrs.2018.e00197.
Mota, J.C.A., Silva, C.P., Almeida, B.G., Romero, R.E., Alencar, T.L. de, Lobato, M.G.R., Oliveira, L. de S., Souza, L. da S., Costa, M.C.G., 2021. Cohesive character in Alfisols, Ultisol and Oxisols in Northeast of Brazil: Relationship of tensile strength with silicon, aluminum and iron from poorly crystalline compounds. Geoderma Reg. 24, e00361 https://doi.org/10.1016/j.geodrs.2021.e00361.
Nascimento, Í.V., Fregolente, L.G., Pereira, A.P. de A., Nascimento, C.D.V., Mota, J.C.A., Ferreira, O.P., Sousa, H.H. de F., Silva, D.G.G., Simões, L.R., Souza Filho, A.G., Costa, M.C.G., 2023. Biochar as a carbonaceous material to enhance soil quality in drylands ecosystems: A review. Environ. Res 233, 116489. https://doi.org/10.1016/j.envres.2023.116489.
Oliveira, L.G.L., Ipiranga, A.S.R., 2011. Evidences of the sustainable innovation in the cashew agribusiness context in Ceará - Brazil. Rev. De. Adm. ção Mackenzie 12, 122–150. https://doi.org/10.1590/S1678-69712011000500006.
Oliveira, L.S., Maia, R.N., Assis Júnior, R.N., Romero, R.E., Costa, M.C.G., Alencar, T.L., Mota, J.C.A., 2020. Tensile strength values for the degrees of soil consistency using human perception and TS-Soil device. Catena (Amst.) 190, 104541. https://doi.org/10.1016/j.catena.2020.104541.
Or, D., Ghezzehei, T.A., 2002. Modeling post-tillage soil structural dynamics: a review. Soil Tillage Res 64, 41–59. https://doi.org/10.1016/S0167-1987(01)00256-2.
Pértile, P., Reichert, J.M., Gubiani, P.I., Holthusen, D., Costa, A. da, 2016. Rheological Parameters as Affected by Water Tension in Subtropical Soils. Rev. Bras. Cienc. Solo 40. https://doi.org/10.1590/18069657rbcs20150286.
Pértile, P., Holthusen, D., Gubiani, P.I., Reichert, J.M., 2018. Microstructural strength of four subtropical soils evaluated by rheometry: properties, difficulties and opportunities. Sci. Agric. 75, 154–162. https://doi.org/10.1590/1678-992x-2016-0267.
Queiroz, A. dos S., Dias, C.T. dos S., Lopes, A. da S., Nascimento, Í.V., Oliveira, L. de S., Almeida, B.G., Araújo Filho, J.C., Souza, L. da S., Silva, M.B., Romero, R.E., Toma, R. S., Sousa, H.H. de F., Mota, J.C.A., 2023. Water content as a deterministic factor in the assessment of cohesive character in soils of Coastal Tablelands (Northeast, Brazil). Geoderma Reg. 32, e00600 https://doi.org/10.1016/j.geodrs.2022.e00600.
Reichert, J.M., Suzuki, L.E.A.S., Reinert, D.J., Horn, R., Håkansson, I., 2009. Reference bulk density and critical degree-of-compactness for no-till crop production in subtropical highly weathered soils. Soil Tillage Res 102, 242–254. https://doi.org/10.1016/j.still.2008.07.002.
Reichert, J.M., Rosa, V.T., Vogelmann, E.S., Rosa, D.P., Horn, R., Reinert, D.J., Sattler, A., Denardin, J.E., 2016b. Conceptual framework for capacity and intensity physical soil properties affected by short and long-term (14 years) continuous no-tillage and controlled traffic. Soil Tillage Res 158, 123–136. https://doi.org/10.1016/j.still.2015.11.010.
Reichert, J.M., Brandt, A.A., Rodrigues, M.F., Reinert, D.J., Braida, J.A., 2016a. Load dissipation by corn residue on tilled soil in laboratory and field-wheeling conditions. J. Sci. Food Agric. 96, 2705–2714. https://doi.org/10.1002/jsfa.7389.
Reichert, J.M., Mentges, M.I., Rodrigues, M.F., Cavalli, J.P., Awe, G.O., Mentges, L.R., 2018. Compressibility and elasticity of subtropical no-till soils varying in granulometry organic matter, bulk density and moisture. Catena (Amst.) 165, 345–357. https://doi.org/10.1016/j.catena.2018.02.014.
Reichert, J.M., Corcini, A.L., Awe, G.O., Reinert, D.J., Albuquerque, J.A., García, C.C.G., Docampo, R., 2022. Onion-forage cropping systems on a Vertic Argiudoll in Uruguay: Onion yield and soil organic matter, aggregation, porosity and permeability. Soil Tillage Res 216, 105229. https://doi.org/10.1016/j.still.2021.105229.
Ribeiro, M.R., 2001. Características morfológicas dos horizontes coesos dos solos dos Tabuleiros Costeiros. Workshop Coesão Em Solos Dos Tabuleiros Costeiros. Embrapa, Aracaju, pp. 161–168.
Santos, H.G., Jacomine, P.K.T., Anjos, L.H.C., Oliveira, V.A., Lumbreras, J.F., Coelho, M. R., Almeida, J.A., Araújo Filho, J.C., Oliveira. J.C., Cunha, T.J.F., Jarbas Ferreira Cunha, T., 2018. Sistema Brasileiro de Classificação de Solos, 5th ed. Embrapa, Brasília.
Savant, N.K., Korndörfer, G.H., Datnoff, L.E., Snyder, G.H., 1999. Silicon nutrition and sugarcane production: A review. J. Plant Nutr. 22, 1853–1903. https://doi.org/10.1080/01904169909365761.
Seifu, W., Elias, E., 2018. Soil Quality Attributes and Their Role in Sustainable Agriculture: A Review. Int J. Plant Soil Sci. 26, 1–26. https://doi.org/10.9734/ijpss/2018/41589.
Silva, A.P., Kay, B.D., Perfect, E., 1994. Characterization of the Least Limiting Water Range of Soils. Soil Sci. Soc. Am. J. 58, 1775–1781. https://doi.org/10.2136/sssaj1994.03615995005800060028x.
Sobucki, V., Holthusen, D., Batistão, A.C., Mota, J.C.A., Reichert, J.M., 2022. Potential of rheometry in detecting cohesive soils in Brazil as an additional tool to morphological field description and tensile resistance quantification. Geoderma Reg. 30, e00553 https://doi.org/10.1016/j.geodrs.2022.e00553.
Soil Survey Staff, 2022. Keys to Soil Taxonomy, 13th ed. United States Department of Agriculture, Natural Resources Conservation Service.
Sokołowska, Z., Szewczuk-Karpisz, K., Turski, M., Tomczyk, A., Cybulak, M., Skic, K., 2020. Effect of Wood Waste and Sunflower Husk Biochar on Tensile Strength and Porosity of Dystric Cambisol Artificial Aggregates. Agronomy 10, 244. https://doi.org/10.3390/agronomy10020244.
Sommer, M., Kaczorek, D., Kuzyakov, Y., Breuer, J., 2006. Silicon pools and fluxes in soils and landscapes—a review. J. Plant Nutr. Soil Sci. 169, 310–329. https://doi.org/10.1002/jpln.200521981.
Tang, Y., Liu, X., Lian, J., Cheng, X., Wang, G.G., Zhang, J., 2023. Soil Depth Can Modify the Contribution of Root System Architecture to the Root Decomposition Rate. Forests 14, 1092. https://doi.org/10.3390/f14061092.
Tormena, C.A., Silva, A.P., Libardi, P.L., 1998. Caracterização do intervalo hídrico ótimo de um latossolo roxo sob plantio direto. Rev. Bras. Cienc. Solo 22, 573–581. https://doi.org/10.1590/S0100-06831998000400002.
Tormena, C.A., Fidalski, J., Rossi Junior, W., 2008. Resistência tênsil e friabilidade de um Latossolo sob diferentes sistemas de uso. Rev. Bras. Cienc. Solo 32, 33–42. https://doi.org/10.1590/S0100-06832008000100004.
Valadão Junior, D.D., Biachini, A., Valadão, F.C.A., Rosa, R.P., 2014. Penetration resistance according to penetration rate, cone base size and different soil conditions. Bragantia 73, 171–177. https://doi.org/10.1590/brag.2014.013.
Vieira, J.M., 2013. Contribuição de compostos de baixa cristalinidade e ciclos de umedecimento e secagem na gênese do caráter coeso em solos do Ceará (Master's Thesis). Federal University of Ceará, Fortaleza.
Vieira, J.M., Romero, R.E., Ferreira, T.O., Assis Júnior, R.N., 2012. Contribuição de material amorfo na gênese de horizontes coesos em Argissolos dos Tabuleiros Costeiros do Ceará. Rev. Ciência Agron. ômica 43, 623–632. https://doi.org/10.1590/S1806-66902012000400002.
Wang, Y., Xiao, X., Chen, B., 2018. Biochar Impacts on Soil Silicon Dissolution Kinetics and their Interaction Mechanisms. Sci. Rep. 8, 8040. https://doi.org/10.1038/s41598-018-26396-3.
Wang, Y., Xiao, X., Xu, Y., Chen, B., 2019. Environmental effects of silicon within biochar (sichar) and carbon–silicon coupling mechanisms: a critical review. Environ. Sci. Technol. 53, 13570–13582. https://doi.org/10.1021/acs.est.9b03607.
Wang, Y., Zhang, K., Lu, L., Xiao, X., Chen, B., 2020. Novel insights into effects of silicon-rich biochar (Sichar) amendment on cadmium uptake, translocation and accumulation in rice plants. Environ. Pollut. 265, 114772 https://doi.org/10.1016/j.envpol.2020.114772.

Watts, C.W., Dexter, A.R., 1998. Soil friability: theory, measurement and the effects of management and organic carbon content. Eur. J. Soil Sci. 49, 73–84. https://doi.org/10.1046/j.1365-2389.1998.00129.x.

Yang, X., Zhang, S., Ju, M., Liu, L., 2019. Preparation and Modification of Biochar Materials and their Application in Soil Remediation. Appl. Sci. 9, 1365. https://doi.org/10.3390/app9071365.

Zhang, W., Meng, J., Huang, Y., Sarkar, B., Singh, B.P., Zhou, X., Gao, J., Teng, Y., Wang, H., Chen, W., 2023. Effects of soil grain size and solution chemistry on the transport of biochar nanoparticles. Front Environ. Sci. 10 https://doi.org/10.3389/fenvs.2022.1114940.

Zong, Y., Chen, D., Lu, S., 2014. Impact of biochars on swell–shrinkage behavior, mechanical strength, and surface cracking of clayey soil. J. Plant Nutr. Soil Sci. 177, 920–926. https://doi.org/10.1002/jpln.201300596.